Atmos. Chem. Phys. Discuss., 14, 21223–21283, 2014
www.atmos-chem-phys-discuss.net/14/21223/2014/
doi:10.5194/acpd-14-21223-2014

Atmospheric Chemistry and Physics Discussions

Importance of aerosol composition and mixing state for cloud droplet activation in the high Arctic

C. Leck and E. Svensson

Department of Meteorology and Bert Bolin Centre for Climate Research, Stockholm University, 10691 Stockholm, Sweden

Received: 15 April 2014 – Accepted: 1 August 2014 – Published: 19 August 2014

Correspondence to: C. Leck (lina@misu.su.se)

Published by Copernicus Publications on behalf of the European Geosciences Union.

Abstract

Concentrations of cloud condensation nuclei (CCN) were measured throughout an expedition by icebreaker around the central Arctic Ocean, including a 3 week ice drift operation at 87° N, from 3 August to 9 September 2008. In agreement with previous observations in the area and season median daily CCN concentrations at 0.2 % water vapor supersaturation were typically in the range of 15 to 30 cm^{-3}, but concentrations varied by two to three orders of magnitude over the expedition and were occasionally below 1 cm^{-3}. The CCN concentrations were highest near the ice edge and fell by a factor of three in the first 48 h of transport from the open sea into the pack ice region. For longer transport times they increased again indicating a local source over the pack ice, suggested to be polymer gels, via drops injected into the air by bubbles bursting on open leads. By assuming Köhler theory and simulating the cloud nucleation process using a Lagrangian adiabatic air parcel model that solves the kinetic formulation for condensation of water on size resolved aerosol particles we inferred the properties of the unexplained non-water soluble aerosol fraction that is necessary for reproducing the observed concentrations of CCN. We propose that the portion of the internally/externally mixed water insoluble particles was larger in the corresponding smaller aerosol sizes ranges. These particles were physically and chemically behaving as polymer gels: the interaction of the hydrophilic and hydrophobic entities on the structures of polymer gels during cloud droplet activation would at first only show a partial wetting character and only weak hygroscopic growth. Given time, a high CCN activation efficiency is achieved, which is promoted by the hydrophilicity or surface-active properties of the gels. Thus the result in this study argues for that the behavior of the high Arctic aerosol in CCN-counters operating at water vapor supersaturations > 0.4 % (high relative humidities) may not be properly explained by conventional Köhler theory.

ACPD
14, 21223–21283, 2014

1 Introduction

Twomey (1974) showed that the state of division of the available water in clouds determines the amount of short wave radiation scattered back to space, the effect being largest in optically thin clouds with few water drops. This is particulate true for Arctic low-level clouds (Walsh et al., 2002; Tjernström et al., 2008). Further these Arctic low-level clouds, while controlling the surface radiation balance, have a pronounced influence on the melting and freezing of the perennial sea ice (Intrieri, 2002; Kay and Gettelman, 2009; Mauritsen et al., 2010; Sedlar et al., 2011). For most of the year, such clouds tend to warm the surface, but during the peak melt season at the end of the summer, low-level clouds could cool the ice surface and thereby influence the timing of the autumn freeze-up. Earlier freeze-up will cause thicker ice that might melt less during the following summer, surviving into the subsequent winter. If such a process were to recur over several years, it could delay or even prevent sea ice from melting completely during the Arctic summer. In other words, it would constitute a negative feedback. The concentration of cloud water drops is largely determined by the concentration of nuclei on which cloud drops can form (cloud condensation nuclei, or CCN). This also requires that the meteorological conditions, wind, humidity and temperature are favorable.

Measurements of cloud condensation number concentrations (CCNC) over the pack ice are scarce due to the remoteness of the area. From research carried out in a series of four international ice-breaker expeditions to the high Arctic in the summers of 1991 (Leck et al., 1996), 1996 (Leck et al., 2001), and 2001 (Leck et al., 2004; Tjernström et al., 2004) and in 2008 (Tjernström et al., 2014) there has been no other effort relevant to the formation of low-level clouds, north of 80° during conditions when influences from man-made particle sources being limited. CCNC have been observed to vary by three orders of magnitude over the period July to September and commonly by an order of magnitude within a day but were usually lower than 100 cm^{-3}, occasionally less than 1 cm^{-3} (Lannefors et al., 1983; Bigg et al., 1996, 2001; Bigg and Leck, 2001a; Leck et al., 2002; Mauritsen et al., 2011). Figure 6 in Mauritsen et al. displays fre-

ACPD
14, 21223–21283, 2014

quency distributions of observed CCNC from all four expeditions measured at different water vapor supersaturations (SS), ranging 0.1 to 0.8 %. All four populations showed an overall consistent distribution with three quarters of the CCNC being greater than 10 cm^{-3} but less that about 100 cm^{-3}, medians typically in the range 15 to 50 cm^{-3} as reported by Bigg et al. (1996) and Bigg and Leck (2001a).

In searching for a relationship between the properties of the summer high Arctic aerosol and its ability to form CCN Zhou et al. (2001) calculated, by assuming equilibrium Köhler theory (Köhler, 1936), CCNC from size distribution data and additional hygroscopic growth information, and by assuming that the calculated CCN particles were composed of ammonium sulfate, sodium chloride and a nearly water-insoluble fraction. The closure study resulted in an over-prediction of the calculated CCNC (more CCN were calculated than measured) of around 30 %. In a separate study on the same CCN data Bigg and Leck (2001a) made the simpler assumption that all particles in the number size distribution were composed of pure ammonium sulfate. Again a similar over prediction resulted as reported by Zhou et al. Sorting the CCN data according to meteorological conditions combined with added information on particle morphology and state of mixture Leck et al. (2002) concluded that other components, probably organics, depressed the nucleating ability of the particles. However, on clear-sky days, there were a majority of occasions on which CCNC were more than predicted from a sulfate composition and the measured size distribution. Since equilibrium Köhler theory cannot take kinetic effects into account, which can cause erroneous results when considering the competition of aerosol particles of different size for water vapor, the cloud nucleation process was in addition simulated with a Lagrangian parcel model (Lohmann and Leck, 2005). The authors found it necessary to invoke a highly surface-active Aitken

ACPD
14, 21223–21283, 2014

mode, assumed to be marine gels[1], externally mixed with a sulfur-containing population in order to explain the observed CCNC over the pack ice.

The Arctic marine or polymer gels have been shown to consist of hydrophilic and hydrophobic segments (Orellana et al., 2011) in agreement with their chemical behavior modeled by Xin et al. (2013). The interaction of the hydrophilic and hydrophobic entities on the behavior of the three-dimensional polysaccharide structures during the cloud droplet activation strongly suggests a dichotomous behavior for polymer gels (Ovadnevaite et al., 2011); an only partial wetting character is seen below 100 % relative humidity (RH) and thus showing only weak hygroscopic growth but at the same time a high CCN activation efficiency is shown, which is promoted by the hydrophilicity or surface-active properties of the gels. Most recently Martin et al. (2011) performed yet another CCN closure study being representative for high Arctic summer conditions. To predict the CCNC, the closure was based on data on average measured from 0.1–0.7 % water vapor SS and κ-Köhler theory (Petters and Kreidenweis, 2007). This approach differed from the previous studies that only used one level of water vapor SS (0.2 %.) in the comparison between measured and modeled CCNC. Further Martin et al. used highly time resolved (average over 5 min) sub-micrometer aerosol bulk chemical compositions (sulfate, nitrate, organics and methane sulfonate) obtained by an aerosol mass spectrometer, see Chang et al. (2011) for details. The authors derived total hygroscopicity parameters by permuting parameter values for the components and the solubility of the organics. The surface tension was assumed to be constant and equal to that of pure water. Consistent with the previous results by Zou et al. (2001) and Bigg and Leck (2001a), the calculations generally tended to over predict the observed CCNC, about

[1]Marine gels or polymer gels are produced by phytoplankton and sea ice algae biological secretions at the sea–air surface interface. The polymer gels are made up of water insoluble, heat resistant, highly surface-active and highly hydrated (99 % water) polysaccharide molecules spontaneously forming 3-dimensional networks inter bridged with divalent ions (Ca^{2+}/Mg^{2+}), to which other organic compounds, such as proteins and lipids, are readily bound (Verdugo, 2012 gives a review).

ACPD
14, 21223–21283, 2014

30–60 % higher than the observed ones for water vapor supersaturation above 0.4 %. As an explanation of their results the authors proposed that the portion of the particles assumed to be made up by internally mixed water insoluble organics, was larger in these smaller sizes ranges. The chemical and physical behavior of marine gels is in good agreement with the CCN closure experiments by Martin et al. (2011). The above discussed opposing CCN-closure results indicate that the observed presence of organic constituents in the aerosol most likely will play an important role in determining the ability of the atmospheric aerosol to act as CCN.

This study is aimed to further reduce some of the uncertainties surrounding the CCN properties promoting/suppressing cloud droplet formation in a marine environment with limited influences from man-made activities. This will be made possible by using the observed sensitivity of measured CCNC on average ranging from 0.1–0.7 % water vapor SS used in Martin et al. (2011) combined with Köhler theory and by simulating the cloud nucleation process using a Lagrangian adiabatic air parcel model that solves the kinetic formulation for condensation of water on size resolved aerosol particles. The simulations were based on the diffusional growth equation, as done by Lohmann and Leck (2005). The CCNC will be predicted from observed aerosol number size distribution data and additional hygroscopic growth information, and by assuming that the calculated CCN particles were composed of a inorganic/organic aerosol system. In the latter case we will use the determined aerosol bulk chemistry obtained from highly size resolved impactor samples to show the extent to which determined water-soluble dimethyl sulfide (DMS) oxidation products, sodium chloride and other inorganic compounds contributed to the CCN population. As a surrogate for the unexplained fraction assumed to be organic in nature we will use various water-soluble, slightly water-soluble and non water-soluble proxy constituents. The simulated CCNC will be compared the observed CCNC, at water vapor SS of 0.1–0.9 %, collected during the Arctic Summer Cloud Ocean Study (ASCOS)[2] onboard the Swedish icebreaker *Oden*

[2]The interdisciplinary program of ASCOS was conducted in the fields of marine biology and chemistry, atmospheric chemistry, oceanography and meteorology with the overall aim to im-

ACPD
14, 21223–21283, 2014

in 2008 in the open waters and marginal ice zone of the Greenland Sea–Fram Strait area and over the pack ice north of 80°.

2 Rout of the expedition and measuring systems and methods

2.1 Rout and platform

The CCNC simulations presented here utilize measurements carried out onboard the icebreaker *Oden* as part of ASCOS. Samples were collected in surface air over the central Arctic Ocean during the biologically most active summer period. The expedition departed from Longyearbyen, Svalbard on 2 August 2008 (Day Of Year, DOY 215, note the leap year), and headed north for the pack ice of the central Arctic Ocean. There was a transition from the "marginal ice zone" having 20–70 % ice cover and the "pack ice region" having between 80–95 % ice cover. On 12 August (DOY 225) *Oden* was anchored to a large ice floe, slightly north of 87° N, and proceeded to drift with the ice floe for the following three weeks (referred to as the Pack Ice, PI, -drift), until midnight between 1 and 2 September (DOY 245–246). In transit to the ice drift, additional stations were set up at the ice edge and an open water station in the Greenland Sea–Fram Strait area: an open water station (OW-1) on the 3 August 2008 (DOY 216–216.5) (78.2° N; 7.5° E) followed by a station in the marginal ice zone (MIZ-1) starting on the 4 August 2008 (DOY 217.5) (79.9° N; 6.1° E). On the way back from the ice drift, a second marginal ice edge station (MIZ-2) was set up at the ice edge on the 6 September immediately followed by a final open water station (OW-2) ending on the 7th in the Greenland Sea. As several of the instruments were not in use no data from the MIZ2 and OW2 stations are discussed in this study. *Oden* arrived back at Longyearbyen on 9 September (DOY 253). A map of the route with the ice drift magnified is shown in Fig. 1. All times are

prove our understanding of low-level cloud formation and possible climate feedback processes over the central Arctic Ocean. Tjernström et al. (2014) give more details.

ACPD
14, 21223–21283, 2014

reported in Universal Time Coordinate (UTC). The sun was continuously above the horizon of the expedition.

2.2 Particle measurement systems

The measurements utilized in this study were made from a sampling manifold with an impactor (Anderson Inc., Atlanta, Ga) 50 % cutoff diameter of 10 µm (PM_{10}) at 25 m height onboard *Oden*. The PM_{10} inlet was identical to the one used during all three previous expeditions in the summers of 1991, 1996 and 2001. Direct contamination from the ship was excluded by using a pollution controller, turning off all the pumps of the sampler, in direct connection to the sampling manifold. To maximize sampling time safe from pollution our strategy was to keep the sampling manifold facing upwind to avoid sampling of ship exhausts. This necessitated a "harbor" in the ice in which the ship, with its non-rotating mast on the 4th deck, could be moored in several different directions and turned as the wind direction changed. Further details of the location and properties of air intakes and instruments, position on the ship, pumping arrangements and precautions to exclude contaminated periods can be found in Leck et al. (2001) and in Tjernström et al. (2014). Key instruments used and important measurement details are discussed below.

(1) Aerosol particles that are active as CCN were measured continuously using two identical CCN counters (Roberts and Nenes, 2005) operating in parallel. Aerosol particles enter the CCN counter through an inlet at the top and pass through a cylindrical column where they can activate and grow to droplet size. In the column a temperature gradient is established, with the lowest temperature at the top. The walls of this column are wetted with water. Thus, heat and water vapor are transported towards the center of the column by diffusion. As heat diffuses more slowly than water in air in the temperature range used, a constant water vapor supersaturation (SS) is established in the center of the column. This supersaturation can be adjusted by changing the temperature gradient of the column. At the outlet of the column the activated particles are counted with an optical particle counter (OPC) and collected in different size bins. The

ACPD
14, 21223–21283, 2014

CCN counter defines a CCN as a particle having a wet diameter > 1 µm and a positive growth rate. The CCN counter undercounts particles if they have not grown larger than 1 µm by the time they reach the OPC.

The first CCN counter was set to a constant water vapor SS of ca. 0.2 % averaged over one minute, which was slightly increased later for better comparison with CCN data collected during three former expeditions: measurements were performed at 0.17 % SS between 3 August (DOY 216) to 15 August (DOY 228) and at 0.21 % SS for the remaining period 16 August (DOY 229) to 9 September (DOY 253). The second counter scanned five different water vapor SS on average: 0.10 (0.082–0.106), 0.15 (0.126–0.161), 0.20 (0.171–0.233), 0.41 (0.347–0.521), 0.73 (0.613–0.952) percent with a measurement period of 30 min each. This enabled a determination of the sensitivity of measured CCN to the choice of water vapor SS. Martin et al. (2011) give more information on the quality and data processing of the CCNC measurements.

(2) Aerosol particle number size distributions at 10 to 20 min time resolution were measured in 45 bins from 3–800 nm in diameter using a Twin Differential Mobility Particle Sizer (TDMPS; Birmilli et al., 1999). Throughout this paper all number particle sizes will be referred to as dry geometric mean diameters (GMD). Further details on the quality and data processing of these measurements are available in Heintzenberg and Leck (2012).

(3) To measure the growth of individual particles in diameter sizes of 31, 50, 72, 108, 163 and 263 nm from the dry state (< 20 % RH) to a set RH, an H-TDMA (Hygroscopic Tandem Differential Mobility Analyzer) instrument was used. Zhou et al. (2001) gives details.

(4) Aerosol bulk chemical composition was determined from a 13 stage (30 $dm^3\,min^{-1}$), LPI (Dekati, http://dekati.com/cms/) impactor. Upstream of the impactor, the temperature and the RH of the incoming sample air were measured and recorded using mini probes and a data acquisition system custom made for the expedition by Vaisala. The LPI impactor had 50 % cut off diameters of: 10.0, 6.57, 3.96, 2,45, 1,60, 0.990, 0.634, 0.391, 0.253, 0.165, 0.104, 0.060 and 0.029 aerodynamic di-

ACPD
14, 21223–21283, 2014

ameter (EAD). Polycarbonate collection foils were used as the collection substrate. To avoid super-micrometer particles bouncing off, Polycarbonate stages 1–3 were greased (Apiezon-L dissolved in acetone).

Blank levels were determined by loading the impactor with the substrates at the sampling site for the length of the sampling period but with no air drawn through it. The detailed size segregated LPI impactor required relative long sampling times of 20–40 h resulting in 18 sampling periods obtained during the course of ASCOS.

2.3 Water soluble mass determination

To allow for subsequent chemical determinations all substrates, ambient samples and blanks were carefully handled in a glove box (free from particles, sulfur dioxide and ammonia) both prior to and after sampling. At the time of the chemical analyses, still in the glove box, the substrates were extracted (in centrifuge tubes) with 5 cm^3 deionized water (Millipore Alpha-Q, conductivity 18 MΩcm). For sufficient extraction the substrate extracts were finally placed in an ultra sonic bath for 60 min. The extracts were then analyzed for major cations, anions and weak anions by chemically suppressed ion chromatography (IC, Dionex ICS-2000). The anions were analyzed with Dionex AG11/AS11 columns and the cations with CG16/CS16. A Dionex ATC-1 column was used before the injection valve to trap carbonates and other ionic contaminants. The injection volume was 50 µdm^3. Quality checks of the analyses were performed with both internal and external reference samples (organized by EANET, 2008). The analytical detection limits obtained for the various ions, defined as twice the level of peak-to-peak instrument noise, were 0.20, 0.05, 0.10, 0.01, 0.01 and 0.25, 0.02, 0.01, and 0.001 µeqdm^{-3} for ammonium: NH_4^+, sodium: Na^+, potassium: K^+, magnesium: Mg^{2+} and calcium: Ca^{2+}, chloride: Cl^-, MSA: CH_3SOO^-, oxalate: $C_2O_4^{2-}$, nitrate: NO_3^- and sulfate: SO_4^{2-}, respectively. During the expedition LPI levels (sample minus blank) of MSA, Cl^-, NO_3^-, SO_4^2, Oxalate, Na^+, K^+, Mg^{2+} and Ca^{2+} down to 0.002, 0.030, 0.009, 0.010, 0.007, 0.030, 0.004, 0.008, and 0.032 nmol m^{-3}, respectively were detected.

ACPD
14, 21223–21283, 2014

2.4 Air trajectories and time spent over the pack ice

The vertical structure of the atmosphere was typical for central Arctic summer during the expedition. The air layer closest to surface was shallow and well mixed with depths usually below 200 m. This layer was capped by a temperature inversion with a stable stratification of the atmosphere aloft due to the advection of warmer air from the south (Tjernström et al., 2012). The backward trajectories were calculated[3] for an arrival height in the well-mixed layer within the ABL, 100 m a.s.l., at hourly intervals. The height of 100 m is a compromise to ensure that at least the receptor point is fairly close to the surface where the samples were collected (25 m a.s.l.), and at least in the well-mixed layer but also that trajectories, due to rounding errors and interpolation, would not run too great a risk to "hit the surface" in the backward trajectory calculations. To use *Oden*'s position as a starting point of the backward trajectory calculations gave a point that is very precisely measured with GPS. Backward trajectories have several sources of uncertainty, which generally grows with the length of the trajectory. Most uncertain is transport in the vicinity of strong gradients, such as frontal zones, while within a single air mass the trajectory calculations are likely more reliable.

With the help of the back-trajectories and ice maps[4] the time elapsed since the air was last in contact with the open ocean was computed in the way that Nilsson (1996) reported. It will be referred to as days over ice (DOI). The calculated DOI thus marks the end point for an air parcel that left the ice edge between 0–10 days ago (resolved

[3]The NOAA HYSPLIT (Hybrid Single-Particle Lagrangian Integrated Trajectory) model (Draxler and Rolph, 2011; Rohph, 2011) was used to calculate three-dimensional five and ten day backward trajectories of the air reaching *Oden*'s position. The trajectory calculations were based on data from the Global Data Assimilation System (GDAS) of the National Weather Service's National Center for Environmental Prediction (NCEP). Vertical motion in the trajectory runs was calculated using the model's vertical velocity fields.

[4]Ice maps from Satellite-sensor, AMSR-E, "level 1A" with the data sourced from NSIDC (Boulder), United States, finalized at Bremen University, http://iup.physik.uni-bremen.de:8084/amsr/amsre.html were used.

ACPD
14, 21223–21283, 2014

by the length of the trajectories). The measure of DOI will in the later analyses be used as a simple parameter to summarize the evolution of the aerosol as a function of the synoptic scale systems since their last contact with open sea. Calculated cumulative travel times over ice for ASCOS, showed that most trajectories spent at least three days (median 3.3 days) over the pack ice before reaching *Oden*. Travel times less than two days were encountered around 30 % and travel times of four days and longer covered about 40 % of the cases.

3 Computional methodes

Köhler (1936) describes the relationship between chemical properties, size and water vapor supersaturation present at the surface of an aerosol droplet in thermodynamic equilibrium. The Köhler theory consists of the Kelvin effect, which describes the influence on water vapor SS pressure from the curvature of the spherical surface of an aerosol droplet, and the Raoult effect, which represents the influence from the solute. One key parameter in the Kelvin term is the surface tension. The surface tension of an aerosol particle is not only influenced by the curvature of the droplet but also determined by the concentration of amphiphilic solutes (Hede et al., 2011). Thus inorganic salts could be assumed to have an increasing effect on surface tension due to the ionic interactions, whereas surface-active organic compounds decrease the surface tension due to the amphiphilic properties disturbing the hydrogen bonding at the air/water interface. If a thermodynamic equilibrium with the environment of the aerosol droplet can be assumed the droplet diameter size of a growing CCN particle can be calculated at a specific water vapor SS pressure. In the simplest use of the traditional Köhler theory keeping all parameters constant, the larger the aerosol droplet diameter is, the lower critical water vapor SS pressure is required for final activation into a cloud droplet.

ACPD
14, 21223–21283, 2014

The water vapor SS pressure over an aqueous aerosol droplet can also be expressed to depend on the droplet water activity (a_w) according to:

$$SS = a_w \exp(4\sigma_{s/a} M_w / RT\delta_w D), \quad (1)$$

where $\sigma_{s/a}$ is the surface tension between the solution and air, M_w is the molecular weight of the water solution, δ_w the density of the solution, R is the universal gas constant, T is the absolute temperature and D is the diameter of the droplet at the water vapor SS pressure. The droplet water activity, a_w, is a straightforward parameter, which can be measured directly in laboratory experiments. Svenningsson et al. (2006) measured water activities as functions of solution molality for various mixtures of inorganic and organic compounds, and gave parameterizations. In this study we have used the MIXSEA mixture (ammonium sulfate 50 %, sodium chloride 30 %, succinic acid 10 % and fulvic acid 10 %) parameterization.

The above formula (1) can be reformulated using κ-Köhler theory (Petters and Kreidenweis, 2007). κ-Köhler theory is a one-parameter model, where the solute hygroscopicity parameter, κ, combined with the Kelvin term represents a measure of aerosol droplet water uptake and activity and thus determines the equilibrium water vapor SS over an aqueous droplet. Values of κ for specific constituents, or mixtures thereof, can be determined experimentally. Fitted values of κ for individual aerosol constituents may be combined to represent the hygroscopic behavior of mixed aerosol particles of known composition. The water vapor SS pressure over an aqueous aerosol droplet could is in this case be expressed as:

$$SS = D^3 - D_d^3 / D^3 - D_d^3 (1 - \kappa) \exp(4\sigma_{s/a} M_w / RT\delta_w D), \quad (2)$$

where D_d is the volume equivalent diameter of the dry aerosol particle. κ depends on the water activity of the aerosol droplet and the volumes of the dry particle and of the aerosol droplet. It ranges between 0 for water-insoluble particles, and values >1 for very water soluble salts (κ = 1.28 for NaCl). κ of an aerosol droplet is defined as the sum of the products of the κ values of all single solute components, i, in the aerosol

ACPD
14, 21223–21283, 2014

droplet and their corresponding volume fractions $\epsilon_i = V_i/V_{tot}$, thus $\kappa_{tot} = \sum_i \kappa_i \epsilon_i$. To calculate κ_{tot}, κ values and densities for the separate mass constituents measured by the impactors had to be assumed. As with traditional Köhler theory, the maximum in water vapor SS computed for a specified initial dry particle size (referred to as the activation limit dry diameter) and composition (expressed by κ) determines the particle's critical water vapor supersaturation (SSc) for activation to a cloud droplet.

Since equilibrium Köhler theory cannot take kinetic effects into account, which can cause erroneous results when considering the competition of aerosol particles of different size for water vapor, we simulated the cloud nucleation process by assuming Köhler theory combined with a Lagrangian adiabatic air parcel model (coded in Matlab). The model, which is described by Pruppacher and Klett (1997), solves the kinetic formulation for condensation of water on size resolved aerosol particles, based on the diffusional growth equation. The model is composed of essentially the same equations as the model developed in Leaitch et al. (1986) and later applied by Lohman and Leck (2005), but for a few differences. Firstly, due to development of both computer hard- and software it is now possible to solve the full implicit ordinary differential equation system instead of earlier necessary simplifications. Secondly, measured size distributions of both number and chemical compositions are used as direct model input variables. The main advantage of this approach is that the observed mass and number aerosol size distributions are preserved. In the Leitch et al. and Lohman and Leck studies the size distributions had to be transferred to a series of log-normal distributions with constant chemical composition, which caused a risk for loss of size resolved information. However the uncertainty in mass that arises from the chemical analyses together with uncertainties connected with the measured growth factors still could influence our results. Finally, we identify that the Raoult term in the particle growth equation given in the Supplement is equal to $-\ln(a_w)$. Similar to Lohmann and Leck (2005) the model defines a CCN as a particle having a wet diameter $> 1\,\mu m$ and a positive growth rate. The total simulation length was 50 s and set to correspond to the residence time of the

ACPD
14, 21223–21283, 2014

particles in the CCN counter. For more detailed information on the modeling approach we refer to the information in Supplement.

4 Results of CCN measurements

4.1 Temporal changes of CCNC

Figure 2 gives a time series of the observations (averaged over one minute) for water vapor SS of 0.2 % (sampler 1). Blue dots show CCNC measured at 0.17 % SS (DOY 217–228), while light blue dots show the CCNC at 0.21 % SS (DOY 229–253). Between days 216 and 217 all the measurements were collected in the open sea or at the marginal ice edge of the Greenland Sea–Fram Strait area. The period between DOY 225 to 246 represents the ice drift period. Four features stand out: the CCNC were constantly below 100 cm^{-3} both in the marginal over the pack ice, and occasionally below 1 cm^{-3} (described in Mauritzen et al., 2010), the 2–3 orders of magnitude overall range in concentrations from below 1–100 cm^{-3} and changes in concentration, sometimes exceeding the entire seasonal variation, often occurred within an hour. This large time variability in the data is consistent with measurements from earlier high Arctic campaigns. Work by Bigg et al. (2001) has shown that the common stratification together with dynamic processes within the lower part of the boundary layer exert large influences on near-surface concentrations of aerosols in the central Arctic.

Median daily concentrations were typically ranging 15–30 cm^{-3} but were a factor of 3 higher at the ice edge at latitude 80° N (days 216–217). At the location of the PI-drift station on day 244–245 the median concentration was a factor of 100 lower than on days 216–217, so a temporal change throughout the mouth of August of this magnitude may be buried in the noisy data. However, transport time from open water over the pack ice (referred to as DOI) is shown below to be important and may emphasize the temporal change.

ACPD
14, 21223–21283, 2014

4.2 CCNC changes with DOI and air mass origin

It has become clear from the above discussion that understanding the occurrence of CCNC in the atmosphere over the pack ice will also require an understanding of the synoptic scale systems advecting heat, moisture, and particles from the surrounding open seas for a variable length of time over the pack ice.

Based on the availability of data from key instruments utilized in this study the following group of the impactor samples was included for further analyses, namely OW-1, MIZ-1, PI-1, PI-3, PI-6, PI-8, PI-9, PI-10, PI-13 and PI-15. Their start and stop times are marked in Fig. 2. Table 1 gives more information on start–stop times and sample duration. The observed CCNC were averaged over the impactor sampling times and Table 1 tabulates the 25th, 50th (median) and 75th percentile CCNC separately for open water (OW-1), marginal ice zone (MIZ-1) and pack ice (PI-1, 3, 6, 8, 9, 10, 13, and 15) measurements at 0.2 % SS (counter 1).

Subjective clustering of the backward trajectories for a receptor point of 100 m at the location of the ship (Fig. 3) allowed for an identification of impactor samples representing similar source regions. The origin of the air during both the 1st (PI-1 and PI-6) and 2nd (PI-3, PI-9 and PI-10) clusters was highly variable on a daily basis as of the very synoptically active period during the first half of the expedition (Tjernström et al., 2012). The air trajectories of cluster 1 (Fig. 3a) originated easterly from the Barents and Kara Seas. For cluster 2 (Fig. 3b), they came from the Fram Strait–Greenland Sea area. In both clusters the air spent a relatively short time over the ice (DOI ~ 2) since last contact with open sea. The period of trajectory cluster 1 (PI-1 and PI-6) and part of cluster 2 (PI-3) had numerous melt ponds on the ice surface, with temperatures around 0 °C. The ice-melt was followed by a drop in temperature to −6 °C for about 2.5 days and included the 3rd trajectory cluster (PI-8). The air origin during the 3rd cluster was mainly from Greenland (Fig. 3c). The vertical component of the air trajectories (not presented) shows a subsiding pathway from the free troposphere across Greenland to the surface, which suggests that the air sampled onboard *Oden* was of free tropospheric origin. As

ACPD
14, 21223–21283, 2014

in this case the trajectories did not have any contact with the open sea no DOI could be calculated. After this brief snap shot of cold air near-surface temperatures became semi stationary around −2 °C and hosted part of the 2nd trajectory cluster (PI-9 and PI-10). During the 4th (PI-13) and 5th (PI-15) clusters, Fig. 3d and e, the air flow was largely from north western circumpolar over the pack ice for approximately DOI = 8 and from the direction of the Laptev and East Siberian Seas towards the end of the period but still with no close contact with open sea. The conditions during the 4th trajectory cluster were governed by a persistent stratocumulus layer that contributed to maintain the temperatures between −2 to −3 °C. The 5th trajectory cluster started on 31 August (DOY 244) and ended on 2 September (DOY 246) as the persistent stratocumulus layer went away and the clouds, if present, became optically thin (Mauritsen et al., 2010), which resulted a drastic drop in temperature to −12 °C and sunny conditions. During the OW-1 (DOY 216–217) we experienced air predominantly from the ice-covered archipelago north of Canada and Alaska. The trajectories during OW-1 did not, within 10 days, have any contact with the open sea before entering the pack ice. Therefore also in this case no DOI was calculated. During MIZ-1 (DOY 217–218) the air had a similar path but crossed open water along the east coast of Greenland prior to sampling at the location of the ship.

Figure 4 translates the time series of Fig. 2 and Table 1 into CCNC as a function of the synoptic scale systems since their last contact with open sea, defined as DOI. Perhaps the most important result contained in Fig. 4 is the loss of CCN approaching a factor of 3 during about the first two days of transport from the ice edge, followed by a recovery. Herman and Goody (1976) have modeled the formation of fog and cloud in warm moist air during advection over the pack ice. They concluded that advection fog formed on the first and second day over the pack ice but lifted to form low stratus on day 3. Losses of CCN to the surface in the surface mixed layer will therefore be expected to be at a maximum on the first and second day when drizzle and fallout of fog drops aid deposition to the surface, consistent with the steep decline seen in Fig. 4 and with previous reported studies in the same area and season (Bigg and Leck,

ACPD
14, 21223–21283, 2014

2001a). Thereafter losses should have continued by wet deposition at a lower rate, but we actually see an increase in two of the three impactor samples (IP-6 and IP-13, Table 1) for DOI > 4. This feature is indicative of a source of CCN particles in the inner Arctic as also the results of other independent analyses suggested before (Bigg and Leck, 2001a; Heintzenberg and Leck, 2006; 2012; Kerminen and Leck, 2001; Leck and Bigg, 1999, 2005a, 2010; Leck et al., 2002). In general, primary marine biogenic local sources over the pack ice, in combination with upstream boundary layer transport of precursor gases from the MIZ, was concluded by the previous studies to constitute the origin of CCN particles in air that spent long time over the ice.

One other much less frequently occurring (a few days out of 40 days expedition in total) possible cause of the CCNC increase, represented by sample PI-13 (DOI = 6.1, Table 1), is coinciding with the re-coupling and turbulent mixing between a shallow (~ 150 m deep) surface-based mixed-layer and with a separate mixed layer located in the upper part of the boundary layer – the upper half of which contained stratocumulus clouds (more details in Shupe et al., 2013). Backward trajectory analysis shown in Fig. 3d suggests that the air in the upper boundary layer had come from the Canadian archipelago while that in the lowest 100 m had been over the ice for at least 10 days. Based on the CCN fingerprint we therefore speculate that the surface air that mixed with the upper part of the boundary layer was influenced by continental sources. Several studies from ASCOS support this finding and indicate the presence of continentally sourced air in the boundary layer during the same time period (Paatero et al., 2009; Chang et al., 2011; Leck et al., 2013; Kupiszewski et al., 2013; Sierau et al., 2014).

The extremely low CCNC observed during PI-15 (DOI = 9.3, Table 1) is related to the meteorological conditions (Fig. 3e) and aerosol stratification prevailing during the time of sampling of PI-15. Based on the helicopter profiles observed during ASCOS, Kupiszewski et al. (2013) reports on concentrations of aerosol particles > 300 nm in diameter, used as a proxy for CCN, being very low within the lowermost few hundred metres, with CCNC usually below 0.5 cm^{-3}. The TDMPS measurements onboard *Oden* also showed a strong decrease in CCN-sized particle concentration starting on

ACPD
14, 21223–21283, 2014

the second half of 31 August, confirming the flight observations. The low aerosol particle concentrations were accompanied by an almost complete disappearance of clouds, which was observed from ca. 20:00 UTC on 31 August. Mauritsen et al. (2011) hypothesize that the cause of the tenuous cloud regime is that when the CCNC fall below some critical value, droplets grow large and rapidly sediment out. This contributes both to keeping the CCNC low, by the removal of the CCN, and to remove cloud water, thus keeping the clouds optically thin. An analysis of corresponding CCN data from the previous three *Oden*-based expeditions (Mauritsen et al., 2011) indicates that this tenuous cloud regime could be quite frequent during the Arctic summer, occurring about 25 % of the time.

5 The sensitivity of CCNC as a function of water vapor supersaturations

5.1 Measured CCNC as a function of water vapor supersaturations

Figure 5 displays the sensitivity of measured CCNC (averaged over the duration of each of the impactor samples) as a function of the five levels of water vapor SS (on average 0.10, 0.15, 0.20, 0.41, 0.73 %) seen by the second CCN counter. Increasing the water vapor SS from 0.1 to 0.2 % resulted in a significant increase in CCNC for all impactor samples, but further SS increases resulted in small or non-existent change in CCNC for samples PI-1, PI-3, PI-6, PI-9, PI-10 and PI-13, respectively. This feature was also seen in Sample PI-15 but at a much lower absolute level.

Figure 6 displays the variation in CCNC with increasing water vapor SS normalized to the average values for the duration of each of the impactor samples. The similarity in the shape of CCNC as a function of SS is seen for the PI-1, PI-3, PI-6, PI-9, PI-10, PI-13 and PI-15 impactor samples (Fig. 6 lower panel). It should be noted that the temporal variability in CCNC covered by each of the impactors is high (Fig. 2 and Table 1) and since the measurements for each SS only cover about 20 % of the time within the start and stop times of the impactors systematic biases could result. However, since

ACPD
14, 21223–21283, 2014

all the six samples are showing similar features there is no evident reason to suspect systematic biases. The open water and marginal ice zone samples (OW-1 and MIZ-1) pictured in Fig. 6 (upper panel), show on the other hand, a more or less continuous increases in CCNC with increasing water vapor SS. Only one sample (PI-8) out of all samples collected in the pack ice showed a similar continuous increase in CCNC with increasing water vapor SS.

In view of the observed sensitivity of measured CCNC as a function of water vapor SS the characteristics of the impactor samples could be summarized as follows: (i) OW-1 and MIZ-1 with a with more or less continuously increase in CCNC:s increasing water vapor SS. The air origin was predominantly from the ice covered archipelago north of Canada and Alaska, (ii) pack ice sample PI-8 with a similar feature as of (i). Sample PI-8 collected air with possible free tropospheric origin (cluster 3: Fig. 3c), (iii) samples PI-1, PI-3, PI-6, PI-9, PI-10, PI-13 and PI-15 showing a small or non-existent continuous change in CCNC with increasing water vapor SS $>0.2\,\%$. One common feature for most of these impactor samples is that the sampled air spent a relatively short time over the ice (DOI ~ 2) since last contact with open sea. The origin of the air during PI-1 and PI-6 (trajectory cluster 1: Fig. 3a) and PI-3, PI-9 and PI-10 (cluster 2: Fig. 3b) were easterly from the Barents and Kara Seas and from the Fram Strait–Greenland Sea area. However, for the PI-13 (cluster 4: Fig. 3d) and PI-15 (cluster 5: Fig. 3e) samples, the air was advected over the pack ice for more than 6 days with no close contact with open sea. At first sight the above results suggest that either differences in time of advection of the air over the pack ice, were additional primary marine aerosol sources and atmospheric gas-phase and aerosol dynamical processes could change the properties of the CCN prior to collection, or possible impact from non natural aerosol sources did have any systematic affect on the sensitivity of observed CCNC as a function of water vapor SS.

In searching for a relationship between the properties of the summer high Arctic aerosol and its ability to form CCN the sensitivity of measured CCNC as a function of the five levels of water vapor SS will be predicted from observed aerosol number size

ACPD
14, 21223–21283, 2014

distribution data, additional hygroscopic growth information, and determined aerosol bulk chemistry resolved over size. In the sections to follow we will focus mainly on five samples as representatives for the features summarized above: MIZ-1, PI-1 (trajectory cluster 1), PI-8 (trajectory cluster 3), PI-10 (trajectory cluster 2) and PI-15 (trajectory cluster 5).

5.2 κ-Köhler theory predictions

Evidently the observations discussed above resulted in a significant increase in CCNC for all impactor samples when increasing the water vapor SS from 0.1 to 0.2 %, but further SS increases resulted in a continues, small or non-existent change in CCNC. We next applied κ-Köhler theory (Petters and Kreidenweis, 2007) in order to predict the aerosol activation limit dry diameter as a function of the five SSc levels ranging from 0.1–0.8 % seen by the CCN counter 2. The calculations used κ-values and densities based on a constant aerosol chemical composition derived from the analytical determinations and observed hygroscopic growth factors. The prediction for each of the impactor samples was compared with experimental results of κ and $\sigma_{s/a}$ (Petters and Kreidenweis, 2007). The experimental κ-values ranged from 0.1 to 1. As κ-values of 0.1 or lower were not realistic, based on the impactor chemical composition, κ-values below 0.1 was not included in the comparison. The aerosol surface tension was assumed both to be constant and equal to that of pure water ($\sigma_{s/a} = 73\,\mathrm{mN\,m^{-1}}$ at 20 °C) and to a value of $\sigma_{s/a} = 50\,\mathrm{mN\,m^{-1}}$ representing a case of moderate particle surface activity.

Figure 7 shows that the prediction of the aerosol activation limit dry diameter generally tended to be larger then the expected diameters from the experimentally established pair of κ-and $\sigma_{s/a}$ values. At lower water vapor SSc and in general for impactor samples MIZ-1, PI-1 and PI-8, the mismatch was less severe. The predictions show clearly that impactor PI-10 and PI-15 deviates the most from the experimental results

ACPD
14, 21223–21283, 2014

with a shown increase of the hydrophobic character in the activated particles with decreasing diameter.

To further study the CCN properties apparently suppressing cloud droplet formation with decreasing diameter we will next simulate cloud nucleation assuming Köhler theory combined with the Lagrangian adiabatic air parcel model that solves the kinetic formulation for condensation of water on size resolved aerosol particles. For details on the approach we refer to the Supplement. In Sect. 8 the CCNC simulations will use the observed aerosol number size distribution data and assumptions on the composition on the inorganic/organic aerosol system resolved over size. In the later case the water-soluble determined impactor data will be used together with a best guess of the properties of the "missing non water-soluble fraction", that is the fraction of particles not classified by the chemical determinations. Before presenting the results from the CCNC simulations in Sect. 8, Sects. 6 and 7 will discuss how to assume the "missing non-water soluble" aerosol fraction using a comparison between the TDMPS number size distribution and the converted total water-soluble mass determined by the impactors.

6 Size resolved aerosol water soluble chemical composition by number

The size resolved chemical mass concentration was converted to a chemical number size distribution by firstly transpose the LPI impactor 50 % cut off diameters (EAD at 50 % RH) to dry (20 % RH) GMD. Following the assumptions made in Hinds (1999) and Tang and Munkelwitz (1994) the following dry GMD's resulted: 0.019–0.40 (bin-1), 0.40–0.71 (bin-2), 0.71–0.116 (bin-3), 0.116–0.181 (bin-4), 0.181–0.284 (bin-5), 0.284–0.466 (bin-6), 0.466–0.732 (bin-7), 0.732–1.19 (bin-8), 1.19–1.82 (bin-9), 1.82–2.95 (bin-10), 2.95–4.91 (bin-11), 4.91–7.59 (bin-12) µm. The calculation used a size dependent particle density (on average 1.35 $g\,cm^{-3}$) in general assuming mixtures of mainly sea salt, ammonium sulfate and MSA with smaller amounts of oxalate, potassium, calcium, magnesium and water similar to those determined on the Polycarbon-

ACPD
14, 21223–21283, 2014

ate collection foils for each of the selected impactors. To reduce the calculated GMD from 50 % to 20 % RH an observed hygroscopic growth factors define of 1.15 was used. Thereafter we interpolated the water-soluble mass composition for each of the impactor bins (1–7) to the TDMPS bins within the 20 to 800 nm diameter size range. Figure 8 displays a comparison between the TDMPS number size distribution and the converted total water-soluble mass determined by the impactors. When the observed total particle concentration in TDMPS number size distribution is larger than for the estimated total number concentration based on the chemical determinations, we call the difference in number of particles the "missing non water-soluble fraction", that is the fraction of particles not classified by the chemical determinations. Figure 9 gives additional details on the ionic contribution of Ca^{2+}, Na^{+}, Cl^{-}, SO_4^{2-} and MSA to the total water-soluble mass determined. In the discussion to follow we will refer to the following modal diameter representation of the observations: the Aitken mode (25–70 nm), the accumulation mode (70–1000 nm) and recently nucleated mode (< 10 nm).

The number size distribution of particles represented by sample PI-10 obtained using the TDMPS shows a strong bimodal distribution (Fig. 8, PI-10), with the Aitken and accumulation modes separated with a Hoppel minimum (Hoppel et al., 1994). This is a shown characteristic for an aerosol population modified by in cloud/fog processing (Hoppel et al., 1986) and sourced over a marine area (Heintzenberg et al., 2004). This then is coherent with the air trajectory cluster (Fig. 3b) originating predominantly from the MIZ of the Fram Strait–Greenland Sea area during this period in foggy conditions typical of the first and second day of advection (1.4 days) over the pack ice. The relative pronounced accumulation mode likely was a result of that precursor gases such as DMS oxidation products, transported within the boundary layer from the MIZ, could have condensed on smaller, Aitken mode particles present over the pack ice (Kerminen and Leck, 2001; Heintzenberg et al., 2006; Heintzenberg and Leck, 2012, Leck and Bigg, 2005b), growing them to CCN sizes and allowing them to be activated into cloud droplets. Activated particles could then be grown via in-cloud aqueous phase oxidation of gases such as sulfur dioxide (SO_2), resulting in release of larger particles following

ACPD
14, 21223–21283, 2014

droplet evaporation (Hoppel et al., 1994). Figure 9 (PI-10) confirms the expected large fraction of the oxidation products of DMS (SO_4^{2-} and MSA) to total analyzed water-soluble constituents in the accumulation mode of sample PI-10.

In a condition when the air has been in very recent contact with the MIZ/open water, a further mechanism would involve the release of accumulation mode primary marine particles (biogenic or sea salt) from the MIZ via bubble bursting (Nilsson et al., 2001; Leck et al., 2002; Bigg and Leck, 2008). The sea salt contribution to accumulation mode of the PI-10 water-soluble aerosol fraction is shown in Fig. 9 (PI-10). Moreover recent results have clearly both qualitatively and quantitatively demonstrated that polymer gels (Bigg et al., 2004; Leck and Bigg, 2005a, 2010; Bigg and Leck, 2008; Orellana et al., 2011; Leck et al., 2013), produced by phytoplankton and sea ice algae biological secretions, could constitute an important source of the biogenic primary particles generated by bubble bursting at the sea–air interface. A contribution of polymer gels to the atmospheric aerosol was reported to be strongest in the biologically active waters of the Greenland Sea–Fram Strait area close to the MIZ relative to the open lead source over the pack ice (Leck et al., 2013). Polymer gels could thus potentially have contributed to the missing non water-soluble fraction seen in Fig. 8c (PI-10).

A similar strong bimodal distribution with the Aitken and accumulation modes separated with a Hoppel minimum is seen in sample MIZ-1 (Fig. 8, MIZ-1). The accumulation mode is however less developed compared to in sample PI-10, which would suggest an aerosol to a lesser extent modified by in cloud processing via in-cloud aqueous phase oxidation of SO_2. Still the sulfur containing both Aitken and accumulation mode (Fig. 9, MIZ-1) likely was a result of pre-existing particle e.g. of gel type that could have acted as a site for condensation of the oxidation products of DMS. As seen in Fig. 9 (MIZ-1) sea salt contributed to the water-soluble fraction in the Aitken and -accumulation mode. The contribution of polysaccharides (building blocks of polymer gels) also from bubble bursting at the air–sea interface marine gels can be seen in Leck et al., 2013 (Fig. 4 middle panel).

ACPD
14, 21223–21283, 2014

The impactor sample PI-15 shares the bimodal characteristics of the sample representatives PI-10 and MIZ-1, but at a much lower absolute number concentration and a wider minimum between the accumulation mode and a sub- Aitken mode, see Fig. 8d. The extremely low CCNC observed during PI-15 was discussed in Sect. 3.2 to be related to the meteorological conditions (Fig. 3e) and aerosol stratification (Kupiszewski et al., 2013) prevailing during the duration of PI-15. Below 10 nm (not shown in Fig. 8, PI-15) was a strong mode of recent nucleated particles observed. Statistical analysis of the aerosol size distribution data recorded in the years 1991, 1996, 2001, and 2008 classified 17 % of the observed time period as similar nucleation events, characterized by the spontaneous appearance of several distinct size bands below 200 nm diameter (Karl et al., 2013). To explain the high Arctic nucleation events the same authors suggested a novel route to atmospheric particle generation that appears to be operative during IP-15. It involves the fragmentation of primary marine polymer gels into the air from evaporating fog and cloud droplets, and is supported by observations (Orellana et al., 2011; Karl et al., 2013; Leck et al., 2013).

The ionic composition of the sub-Aitken mode of sample IP-15 was shown negligible in all other water-soluble constituents but for Ca^{2+} (Fig. 9, PI-15). This observation supports the findings by Orellana et al. (2011), Karl et al. (2013) and Leck et al. (2013) who observed polymer gels in atmospheric samples during the course of PI-15. As these polymer gels are polysaccharides molecules inter-bridged with divalent ions, the dominance Ca^{2+} for the sub-Aitken particle sizes seen in Fig. 9 (PI-15) shows a consistent picture. A similar domination of Ca^{2+} for smaller particles was observed in samples PI-1 and PI-10. Sulfur components and Ca^{2+} dominated the chemical composition of the PI-15 accumulation mode.

The single Aitken mode distribution peaking at 45 nm diameter in PI-8 (Fig. 8, PI-8) suggests an aerosol population sourced in the free troposphere (Leck and Persson, 1996). The air trajectory in Fig. 3c showing a subsiding pathway from the free troposphere via across Greenland to the surface also points to air of free tropospheric origin. The low marine biogenic factor calculated for ASCOS by Chang et al. (2011)

ACPD
14, 21223–21283, 2014

again consistently suggests air arriving at the surface without recent contact with the marine influenced boundary layer. Note the high attribution of Na^+ and Cl^- and Ca^{2+}. This likely free tropospheric origin of PI-8 limits our knowledge aerosol sources and thus on candidates for the missing non water-soluble fraction seen in Fig. 8 (PI-8).

7 Assuming the missing non-water soluble aerosol fraction

Based on each of the impactor samples listed in Table 1, the "missing non water-soluble fraction" not classified by the chemical determinations was on average 54 %. Guided by the size resolved bulk chemical information given in Fig. 9 and bulk chemical and electron microscope analyses resulted not only from ASCOS (Chang et al., 2011; Hamacher-Barth et al., 2013; Karl et al., 2013; Leck et al., 2013; Orellana et al., 2011) but from all three previous expeditions in the summers of 1991, 1996 and 2001 (Bigg and Leck, 2001a, b; 2008; Leck and Persson, 1996; Leck and Bigg, 1999, 2002, 2005a, b; 2010; Leck et al., 2002; Lohman and Leck, 2005) we will assume the sub-Aitken mode particles (Fig. 10a–c) to be made up of externally mixed organically derived small polymer gels with hydrophobic and hydrophilic properties to a various degree (Xin et al., 2013; Orrelana et al., 2011). As the sub-Aitken particles grow, we will assume the particles resulting from deposition of acids/organic vapors on a polymer gel-aggregate (Fig. 10d and e) or typical of a sulfur-containing particle with hydroscopic properties in which any nucleus has become obscured by the surrounding of a sulfate-methane sulfonate-ammonium complex (Fig. 10f). The Aitken mode and smaller accumulation mode below ca 100 nm in diameter will be assumed to be represented by external mixtures of gels and internally mixed sulfur constituents (Fig. 10g) whereas accumulation mode particles at a few hundred nanometers diameter will be assumed to be internal mixtures of gels and sulfur constituents.

Finally, the upper end of the accumulation mode above 200 nm in diameter will be assumed to be internal mixtures resulting from multiple sources, as in Fig. 10h, showing sea salt and a bacterium coated with an organic film and by the concentric rings typical

ACPD
14, 21223–21283, 2014

of droplets of sulfuric acid. In addition film and jet drops could add gel material with salt-free water with or without any attached microorganism, Fig. 10i shows an example of the latter.

As a surrogate for the unexplained fraction assumed to be organic (gels and organic vapors) in nature we will use slightly water-soluble and non water-soluble proxy constituents. As a slightly water-soluble but moderate surface-active dicarboxylic acid we used adipic acid, which has been observed in ambient particulate matter including in the Arctic (Narukawa et al., 2002). Also detected in Arctic aerosol particles (Fu et al., 2009) was cis-pinonic acid, which was chosen as a surrogate for highly surface-active properties of the missing fraction with insignificant lowering of the water activity. Predicting a surface tension of mixtures of ionic solutions with surface-active organics is an ambiguous task. Inorganic components may either enhance or inhibit the surface tension depression caused by surfactants, depending on both concentration and substance (Tuckermann, 2007). Hence, one single best scheme to predict surface tension of mixed aqueous solutions is not likely to exist. In this study, when a non-water soluble missing fraction is present in the samples we set the aerosol surface tension to have a value between solution and air interface to $\sigma_{s/a} = 68\,\mathrm{mN\,m^{-1}}$ for adipic acid (Lohmann and Leck, 2005) and a value of $\sigma_{s/a} = 38\,\mathrm{mN\,m^{-1}}$ in the case of cis-pinonic (Tuckermann, 2007). The surface tension of the internally mixed accumulation mode aerosol was obtained by weighting the surface tension of each soluble constituent by its mass fraction.

Table 2, lists the various assumptions concerning the "missing non water-soluble fraction" used in the modeling, idealized for one size bin of a wet aerosol. The wet aerosol is in general assumed to consist of three more or less non-water-soluble units with known determined water-soluble constituents and 1/3 of dry mass not being determined. Diamonds inside the droplets indicate a water-insoluble fraction. The colour scale of the droplet bulks (from gray to blue) show increasing ionic concentration, equivalent to a lowering of water activity. Orange and red droplet fringes show various degrees of depressions in surface tension, red being the strongest.

ACPD
14, 21223–21283, 2014

For the INSOL simulation the missing fraction is assumed to be either a completely water-insoluble core within the water soluble droplet, which could be for example a gel (Fig. 10d, h), dust, bacterium or soot particle or a sulfur-containing particle in which any gel-nucleus has become obscured by the surrounding of a sulfate-methane sulfonate-ammonium complex (Fig. 10f) was captured.

In the AD (low water-solubility and moderate surface active) and PIN (low water-solubility and highly surface active) cases, particles are resulting from deposition of organic vapors on a polymer gel particles exemplified in Fig. 10e.

When the externally non-water soluble fraction was assumed to be made up by pure adipic and/or cis-pinonic acid (AD_ext and PIN_ext respectively) it mimics the behavior of a polymer gel (Fig. 10b and c; upper left of Fig. 10g; Fig. 10j): with shown interaction of its hydrophilic and hydrophobic entities (Orellana et al., 2001; Xin et al., 2013) and only weak hygroscopic growth of the gels below 100 % RH but at the same time with a shown high CCN activation efficiency, which is promoted by the hydrophilicity or surface-active properties of the gels (Ovadnevaite et al., 2011). The proportion between AD_ext and PIN_ext was linearly combined, assuming for example a 50/50 adipic/cis-pinonic acid external particle mixture.

The SOL assumption only takes the chemically determined water-soluble aerosol fraction in regard. This then represents an externally mixed aerosol with the water-soluble, detected compounds as one part (2/3) and a completely CCN-inactive part (1/3) as the other (Fig. 10a). Chuang (2003) fund that an eternally mixed fraction of ambient aerosol, with very slow water uptake, could account for some observations of particle water uptake that could not be explained with conventional Köhler theory.

8 Predicting CCNC

In the following section, we will present and discuss the results from the simulations in the order of PI-1, PI-8, PI-10, PI-15 and MIZ-1. Figure 11 is a compilation of all simulations. First to be notified is that the modeling result in the PIN case, where the missing

ACPD
14, 21223–21283, 2014

fraction was assumed to behave like an internally mixed cis-pinonic acid; low water-solubility and highly surface active, consistently over predicted the observed CCNC for all five impactor samples. These runs are therefore excluded in the graphs of Fig. 11.

Impactor sample PI-1 collected air that spent on average 2.5 days over the pack since its last contact with the Barents and Kara Seas (Fig. 3a, Table 1). As noted in the above sections, the prevailing foggy condition was probably the cause of the observed bimodal number size distribution (Fig. 8, PI-1), with the Aitken and accumulation modes separated with a Hoppel minimum (Hoppel et al., 1994). Based on the aerosol activation limit dry diameters shown in Fig. 7, scanning at the three lowest water vapor SS (0.10, 0.15, 0.20 %) activated particles within the accumulation mode. For the two highest levels of water vapor SS (0.37 and 0.62 %), particles within the Hoppel minimum down to ca. 60 nm in diameter were activated.

As shown in Fig. 11 (PI-1) the simulation runs including the SOL, AD_ext and PIN_ext assumptions of the non-water soluble missing faction were all able to capture the observed CCNC within ± one standard deviation ranging from 0.10 % to 0.62 % water vapor SS. The shown activation for particles with decreasing diameter argues for a relative increased influence of external mixtures of Fig. 10a–c type particles at the large end tail of the Aitken mode. Also the case AD and INSOL did in general capture the observed CCNC but over predicted the CCNC for the highest level of SS. Hence, the aerosol in the accumulation size range was suggested to be mixtures of the type of particles exemplified in Fig. 10g–i but possibly also of type 10d–f.

Impactor PI-10 collected air originating predominantly from the MIZ of the Fram Strait–Greenland Sea area (Fig. 3b) in foggy conditions typical of the first and second day of advection over the pack ice. Seen in sample PI-10 (Fig. 8, PI-10) was a similar bimodal distribution, as of PI-1, with the Aitken and accumulation modes separated with a Hoppel minimum. The accumulation mode was however more developed (larger and broader). This suggests an aerosol to a greater extent modified by in cloud processing.

ACPD
14, 21223–21283, 2014

Based on the aerosol activation limit dry diameters for PI-10 (Fig. 7) the scanning, with all five water vapor SS (0.10, 0.15, 0.20, 0.41 and 0,73 %) included, activated the accumulation mode particles down to ca. 80 nm diameter.

Similar to IP-1 all assumptions of the non-water soluble missing faction were able to reproduce the observed CCNC within ± one standard deviation below 0.20 % water vapor SS (Fig. 11, PI-10). However all calculations above 0.20 % SS over predicted the observed CCNC. This result indicates that neither using the most conservative assumption on the missing fraction (INSOL: internal mixture with a completely insoluble and non-surface active core) nor using the assumption of an externally mixed aerosol with 2/3 being water-soluble and 1/3 being completely CCN-inactive could predict the sensitivity of the observed CCNC as a function of water vapor SS.

The extremely low, usually below 0.5 cm^{-3}, and highly variable CCNC observed during PI-15 (Fig. 2, Table 1) was as discussed above to be related to the meteorological conditions (Fig. 3e) and aerosol stratification prevailing during the time of sampling of PI-15 (Kupiszewski et al., 2013).

For particle sizes above 10 nm in diameter, shared PI-15 the bimodal characteristics with samples PI-1 and PI-10, but with a wider minimum between the accumulation mode and a sub- Aitken mode (Fig. 8, PI-15). As the low aerosol particle concentrations resulted in an almost complete disappearance of clouds (Mauritsen et al., 2011) and clear sky's during the duration of PI-15 the minimum is primarily not a result of an aerosol population modified by in cloud/fog processing (Hoppel et al., 1986). Being the most pristine case with close to 10 days of advection over the pack ice, the accumulation mode observed during PI-15 is instead likely maintained by polymer gels originating in the surface microlayer (SML, < 1000 µm thick at the air–sea interface) of the high Arctic open leads[5]. It has previously been suggested that the highly surface-active polymer gels could attach readily to the surface of rising bubbles in the water and

[5]The high Arctic open leads can be described as ever-changing open water channels comprising 10–30 % of the ice pack ice area, ranging from a few meters up to a few kilometers in width.

ACPD
14, 21223–21283, 2014

self-collide to form larger aggregates. Before bursting, it was suggested that bubbles stay in the microlayer for some time and therefore are likely to acquire walls, consisting to a large extent of strengthening gels, with embedded particulate matter that may be points of weakness as the water drains from between the walls. Following the burst, the film drop ("film drops": centered on about 100 nm diameter) fragments would not be drops of salt water but of gel material with salt-free water and any particles attached to the fragments. Consequently, polymer gels and their aggregate production, as well as the embedded solid particles such as bacteria, phytoplankton and its detritus can be carried selectively to the surface microlayer by rising bubbles (Bigg et al., 2004; Leck and Bigg, 1999, 2005a, 2010; Leck et al., 2002; Bigg and Leck, 2008). Figure 10i shows an example. Even though jet drop particles ("jet drops": centered around 1 µm diameter) are mainly composed of sea salt, they have over the Arctic pack ice area been observed to be partly coated by polymer gels (Leck et al., 2002). An example is seen in Fig. 10h.

Based on the aerosol activation limit dry diameters for PI-15 (Fig. 7) the CCN-counter activated particles within the accumulation mode between 130 to 200 nm in diameter. According to the results of the simulations presented in Fig. 11 (PI-15), the SOL and AD_ext assumptions gave the best over-all fit to the observed CCNC. It can be argued that the activated fractions of the accumulation mode encompassed an external mixture of particles with internal mixtures of water-soluble constituents strong in DMS- derived sulfur and particles either entirely CCN-inactive, or that the water uptake is impeded and perhaps requires longer than 50 s wetting/growth time in the CCN-counter. The latter properties are consistent with the shown increase of the hydrophobic character in the activated particles with decreasing diameter seen in Fig. 7. In agreement with the observed and modeled chemical behavior of the high Arctic polymer gels with their hydrophilic and hydrophobic segments (Orellana et al., 2011; Xin et al., 2013), water vapor do not uniformly condensate on the gel since only part of the surface exhibits strong hydrophilicity. Thus as discussed above the polymer gels would be expected to show initially only partial wetting character below 100 % RH but given enough time

ACPD
14, 21223–21283, 2014

a high CCN activation efficiency, which is promoted by its surface-active properties (cf. the PIN_ext case in Fig. 11, PI-15) of the gels (Ovadnevaite et al., 2011).

As identified above sample PI-8 was the only sample out of all samples collected in the pack ice with a more or less continuous increases in CCNC with increasing water vapor SS. PI-8 also differed from the above sample in its single Aitken modal number distribution peaking at 45 nm in diameter with a tail into the accumulation mode (Fig. 8, PI-8) causally related to its source in the free troposphere with likely marginal influence from marine sources. Ranging from 0.10 to 0.73 % water vapor SS particles between 50 to 170 nm in diameter were activated (Fig. 7).

As shown in Fig. 11 PI-8, the SOL and AD_ext and PIN_ext assumptions gave the best over-all fit to the observed CCNC but only the PIN_ext case was able to reproduce the measured CCNC within ± one standard deviation for the whole supersaturation range. It can be argued that the activated fractions of the broad Aitken mode encompassed an external mixture of particles with low water-solubility that are highly surface active and internal mixtures of water-soluble constituents.

Impactor sample MIZ-1 showed similar to the samples PI-1, PI-10 and PI-15 a bimodal aerosol number distribution with the Aitken and accumulation modes separated with a Hoppel minimum (Fig. 8, MIZ-1) but exhibited similar to PI-8 a more or less continuous increases in CCNC with increasing water vapor SS.

Based on the aerosol activation limit dry diameters for MIZ-1 (Fig. 7) the range of all five water vapor SS (0.1 to 0.8 %) activated the particles in both the accumulation – and Aitken mode down to ca. 50 nm in diameter.

As seen in Fig. 11 (MIZ-1), none of the simulation cases were able to reproduce the measured CCNC within ± one standard deviation for the whole supersaturation range. For the lowest range of chosen water vapor SS the discrepancy is shown as an under prediction of the observed CCNC whereas quite the opposite is seen for SS above 0.2 %.

ACPD
14, 21223–21283, 2014

9 Modifying the condensation accommodation coefficient

A general conclusion to be drawn from the above simulations is the shown hydrophobic character, which in turn would impend water uptake with decreasing diameter of the aerosol. This was also indicated in the deviation from κ-theory discussed in Sect. 5.

To study this "hydrophobic" feature of the high Arctic aerosol further we added two simulations based on the AD simulation but with a modified condensation accommodation coefficient, α_c. The condensation accommodation coefficient is a quantity characterizing of the behavior of the water molecules in their collisions with the aerosol surface. The value of α_c depends on the surface nature and state as well as on the water vapor supersaturation pressure.

It has been proven to be difficult to determine α_c experimentally. Davis (2006) reports on values varying several orders of magnitude. For pure water and aqueous solutions without surface covers several recent studies indicate that α_c is close to 1 (e.g. Winkler et al., 2004, 2006; Morita et al., 2004). However, several additional studies indicate that water vapor mass transport across the droplet-air interface in atmospheric aerosol may be limited, consistent with a lower value for α_c (e.g. Shantz et al., 2010; Ruehl et al., 2008; Chuang, 2002). Impeding water vapor mass transfer slows down the kinetics and this could result in that the aerosol droplets do not have long enough time to grow to cloud droplet sizes while resident in the CCN counter.

Laboratory studies by Abbatt et al. (2005) showed that thick covers of solid stearic acid were able to shut down the CCN ability of ammonium sulfate particles and attributed this phenomenon to kinetic effects. Takahama and Russell (2011) found, using molecular dynamics simulations, that α_c of a partially covered water surface is roughly equal to the fractional surface coverage. In this study, we tested two different surface coverage scenarios. AC1 has the same properties as the AD case, but with a constantly low $\alpha_c = 10^{-3}$, regardless of both wet and dry particle size. This would correspond to an almost completely covered aerosol droplet with unlimited resources of surface-covering molecules. AC2 shares the properties with AC1 assumption except

ACPD
14, 21223–21283, 2014

that is was assumed that the available surface covering agent is limited so that the every particle has a constant absolute surface area covered. This can be expressed by $\alpha_c = 1 - (D_0/D)^2$ for $D > D_0$ and $\alpha_c = 0$ for $D \leq D_0$, where D is the wet particle diameter and D_0 is a reference diameter. This parameterization makes $\alpha_c = 0$ for small wet diameters and asymptotically approach unity for large wet diameters.

Clearly, there are multiple other choices of parameterizations, which would serve as well, but the data available is not sufficient to distinguish between them. Neither is it possible to unambiguously determine a best value for D_0. Hence, the AC1 and AC2 simulations presented in Table 3 should be viewed as tests of the idea that kinetic effects could reduce the CCN ability as suggested by Abbatt et al. (2005) and Takahama and Russell (2011).

Table 3, lists the new assumptions concerning the "missing non water-soluble fraction" used in the AC1 and AC2 modeling. Black edges indicate surface covers impeding water vapor mass transport across the surface, yielding a lower condensation accommodation coefficient.

The simulation using the AC1 assumption under predicted the observed CCNC within ± one standard deviation for the full range of water vapor SS studied and for all five impactor samples. These simulations are therefore not included in the compilation of the impactor samples shown in Fig. 12.

The AC2 simulation of sample PI-1 was able to capture the sensitivity of the measured CCNC within ± one standard deviation as a function of all the five levels of water vapor SS ranging from 0.1 % to 0.6 %. This argues for that type 10d,e particles, with a limited water vapor mass transport across the droplet-air interface, co-existed with the type 10a–c type of particles at the large end tail of the Aitken mode. The AC2 CCNC simulation as a function of all the five levels of water vapor SS of sample PI-15, represented by the accumulation mode, showed similarly successful (Fig. 12, PI-15). In Sect. 8 above it was argued that the activated fractions of the accumulation mode particles (PI-15) encompassed an external mixture of partly wetted gel-type particles with their shown hydrophobic character and impendent water vapor uptake (be-

ACPD
14, 21223–21283, 2014

ing more dominant with decreasing diameter) with internal mixtures of water-soluble constituents strong in DMS-derived sulfur. This feature of a limited water vapor mass transport across the droplet-air interface of the accumulation mode seems also to be the best possible explanation of the over prediction of CCNC seen for water vapor SS above 0.2 % for PI-10, seen in Fig. 11b.

It was argued based on the simulations shown in Fig. 11 (PI-8) that the activated fractions of the Aitken mode of impactor sample PI-8 encompassed an external mixture of particles with low water-solubility that are highly surface active and internal mixtures of water-soluble constituents. The simulations with modified condensation accommodation coefficients however strongly under predicted the observed CCNC:s at the higher supersaturations, see Fig. 12 (PI-8). Therefore the missing non-water soluble aerosol fraction of the Aitken mode did not show any chemical properties limiting water vapor uptake.

The simulations performed for sample MIZ-1 in Sect. 8 were not at all successful in reproducing the measured CCNC within ± one standard deviation for the whole supersaturation range (broadly activated particles in both the accumulation – and Aitken mode down to ca. 50 nm in diameter): the lowest range of water vapor SS showed an under prediction of the observed CCNC whereas a over prediction was seen for SS above 0.2 %. With the added assumption in the AC2 simulation it was still hard to capture the overall continues increase in observed CCNC with increasing water vapor SS pressures.

We note further that by lowering the D_0 in the AC2 simulation (physically that is equivalent to increasing the available surface coverage area), it seems possible to get a better match. We do however consider this as curve fitting beyond the scope and data available of this study.

ACPD
14, 21223–21283, 2014

10 Summary and conclusions

Concentrations of cloud condensation nuclei (CCN) were measured throughout an ice-breaker expedition (ASCOS) over the central Arctic Ocean, including a 3 week ice drift operation at 87° N, from 3 August to 9 September 2008. Median daily CCN concentrations were typically ranging 15–30 cm^{-3}, being a factor of three higher at the MIZ. The most conspicuous feature of the time series of CCN was the 2–3 orders of magnitude range of concentrations, ranging from below one to 100 cm^{-3}. Highest concentrations occurred over the open water just south of the ice edge in August. Losses of CCN as the air progressed over the pack ice and mixing processes in an often strongly stratified near-surface layer was suggested to contribute most to this large range (Bigg et al., 2001). The losses of CCN (measured at 0.2 % supersaturation) approaching a factor of 3 during the first ca two days in air progressing from the open sea to the pack ice were not surprising in view of the usual evolution of cloudiness that accompanies the progression. It was surprising however that the losses did not continue for longer transport times. A local surface source, presumed to be the bursting of bubbles on the surface of open leads, was suggested in consistency with other previous independent analyses (e.g. Leck and Bigg, 2005a). This open lead source of particles has recently been verified to be biogenic and consist of marine polymer gels (Orellana et al., 2001; Leck et al., 2012).

Previous search for a relationship between the properties of the summer high Arctic aerosol and its ability to form CCN by assuming equilibrium Köhler theory or conventional κ-Köhler theory by Zou et al. (2001), Bigg and Leck (2001a) and Martin el al. (2011), the calculations generally tended to over predict the observed CCNC, about 30–60 % higher than the observed ones for water vapor supersaturation above 0.4 % (Martin et al., 2011). Below 0.2 % water vapor supersaturation in general an excellent agreement was achieved. Further, Lohmann and Leck (2005) found it necessary to invoke a highly externally mixed surface-active Aitken mode in order to explain the observed CCNC over the pack ice.

ACPD
14, 21223–21283, 2014

Intrigued by the above results this study was aimed to further reduce some of the uncertainties surrounding the CCN properties promoting/suppressing cloud droplet formation in a marine environment with limited influences from man-made activities. The main advantage and motivation compare to previous high Arctic CCN-closure studies was the use of water-soluble aerosol bulk chemistry obtained from highly size resolved impactor samples. This enabled us also to make a similar highly size resolved best "guess" of the unexplained number fraction assumed to be organic in nature. Guided by chemical analyses based on electron microscopicity resulting from all three previous expeditions (Bigg and Leck, 2001a, b, 2008; Leck and Bigg, 1999, 2002, 2005a, b, 2010; Leck et al., 2002; Lohman and Leck, 2005) we used various water-soluble, slightly water-soluble and non water-soluble proxy constituents. One further advantage was the possibility to compare the measured and modeled CCNC for more that one set level of water vapor SS, ranging from 0.1–0.8 %. The simulations assumed equilibrium Köhler theory and were based on the diffusional growth equation. In addition calculations were performed using κ-Köhler theory.

This study performed consistent with the previous results by Martin et al. (2011) in that conventional κ-Köhler theory fail to predict the CCNC for samples that had been advected over pack ice. Simulating the cloud nucleation process using a Lagrangian adiabatic air parcel model that solves the kinetic formulation for condensation of water on size resolved aerosol particles at high supersaturation resulted in severe over predictions of the CCNC when even the most conservative assumption on the unknown fraction was used. A general conclusion to be drawn from the CCN simulations and from the calculated deviation from κ-Köhler theory is the shown increase of the hydrophobic character in the activated particles with decreasing diameter. This suggested hydrophobic character of the high Arctic aerosol was also shown by the study of Martin et al. (2011) and would in turn impend water uptake with decreasing diameter of the aerosol.

We tested whether introducing kinetic limitations on water uptake could explain these aerosol properties suppressing cloud droplet activation above 0.4 % water vapor super

ACPD
14, 21223–21283, 2014

saturation. A fixed non-size resolved low water uptake rate consistently produced too low CCNC, but a size dependent assumptions was in general able to capture the sensitivity of the measured CCNC within ± one standard deviation as a function of all the five levels of water vapor SS ranging from 0.1–0.8 %.

The results further suggested that either differences in time of advection of the air over the pack ice, were additional primary marine aerosol sources and atmospheric gas-phase and aerosol dynamical processes could change the properties of the CCN prior to collection, or possible impact from non natural aerosol sources did have any systematic affect on the sensitivity of observed CCNC as a function of water vapor supersaturation. What seems to be of more primary importance is the size resolved state of mixture together with physical and chemical behavior of the fraction of the aerosol population that will undergo droplet activation.

To explain the results we propose that the portion of the internally/externally mixed water insoluble particles, which were physically and chemically behaving as polymer gels, was larger in the corresponding smaller aerosol sizes ranges. The suggestion of the presence of a non-water soluble organic fraction of the CCN population either promoting/suppressing cloud droplet formation thus not deviates from the conclusions drawn by Lohman and Leck (2005) and Martin et al. (2011). The interaction of the hydrophilic and hydrophobic entities on the structures of polymer gels during cloud droplet activation strongly suggests a dichotomous behavior with at first only partial wetting character and only weak hygroscopic growth. Given time, a high CCN activation efficiency is achieved, which is promoted by the hydrophilicity or surface-active properties of the gels (Ovadnevaite et al., 2011). The results in this study argues for that the behavior of the high Arctic aerosol in CCN-counters operating at high relative humilities may not be properly explained by conventional Köhler theory. However, we note that particles with kinetically restricted growth can be activated in real cloud situations even if they are not counted in the CCN counter. It might be that the time (~ 50 s) inside the CCN counter is insufficient for the particles to grow to large enough sizes.

ACPD
14, 21223–21283, 2014

Clearly, there still remain many uncertainties in the evolution of cloud-active particles in the high Arctic and probably elsewhere. One evident outcome from this study is that we have to stop regarding the cloud active particles over remote marine areas to be simply inorganic soluble salts to in addition consist of internal/external mixtures of soluble or slightly soluble organics, which likely will influence the equilibrium water vapor pressure and decrease surface tension of the droplets to be formed. This study also argues for that the Köhler equation used for simulating cloud droplet activation is not fully complete for describing the condensational growth during of the interaction of the hydrophilic and hydrophobic entities on the structures as of the polymer gels suggested to be present at the MIZ and over the pack ice area. For future different approaches are suggested as revisions of the Köhler theory among one is to increase the number of size resolved observations on the morphology, state of mixture and chemical and physical behavior of individual cloud-active particles.

The Supplement related to this article is available online at doi:10.5194/acpd-14-21223-2014-supplement.

Acknowledgements. We greatly thank Maria Martin, Staffan Sjöberg, Douglas Orsini, Berko Sierau, Ulrike Lohmann, Erik Swietlicki, and Jost Heintzenberg for the CCN and aerosol physical data collection and quality assurance work. Jost Heintzenbergs's comments on an early version of the article are appreciated. This work is part of ASCOS (the Arctic Summer Cloud Ocean Study). ASCOS was made possible by funding from the Knut and Alice Wallenberg Foundation and the DAMOCLES European Union 6th Framework Program Integrated Research Project. The Swedish Polar Research Secretariat (SPRS) provided access to the icebreaker *Oden* and logistical support. Michael Tjernström is specifically thanked for his co-coordination of ASCOS. We are grateful to the SPRS logistical staff and to *Oden*'s Captain Mattias Peterson and his crew. ASCOS is an IPY project under the AICIA-IPY umbrella and an endorsed SOLAS project. The Swedish Research Council (VR), the Knut and Alice Wallenberg Foundation and the Bolin Centre for Climate Research at Stockholm University provided support for this work.

ACPD
14, 21223–21283, 2014

References

Abbatt, J. P. D., Broekhuizen, K., and Pradeep Kumar, P.: Cloud condensation nucleus activity of internally mixed ammonium sulfate/organic acid aerosol particles, Atmos. Environ., 39, 4767–4778, 2005.

Bigg, E. K. and Leck, C.: Cloud-active particles over the central Arctic Ocean, J. Geophys. Res., 106, 32155–32166, 2001a.

Bigg, E. K. and Leck, C.: Properties of the aerosol over the central Arctic Ocean, J. Geophys. Res., 106, 32101–32109, 2001b.

Bigg, E. K. and Leck, C.: The composition of fragments of bubbles bursting at the ocean surface, J. Geophys. Res., 113, D11209, doi:10.1029/2007JD009078, 2008.

Bigg, E. K., Leck, C., and Nilsson, E. D.: Sudden changes in arctic atmospheric aerosol concentrations during summer andautumn, Tellus B, 48, 254–271, 1996.

Bigg, E. K., Leck, C., and Nilsson, E. D.: Sudden changes in aerosol and gas concentrations in the central Arctic marine boundary layer: causes and consequences, J. Geophys. Res., 106, 32167–32185, 2001.

Bigg, E. K., Leck, C., and Tranvik, T.: Particulates of the surface microlayer of open water in the central Arctic Ocean in summer, Mar. Chem., 91, 131–141, 2004.

Birmili, W., Stratmann, F., and, Wiedensohler, A.: Design of a DMA-based size spectrometer for a large particle size range and stable operation, J. Aerosol Sci., 30, 549–553, 1999.

Chang, R. Y.-W., Leck, C., Graus, M., Müller, M., Paatero, J., Burkhart, J. F., Stohl, A., Orr, L. H., Hayden, K., Li, S.-M., Hansel, A., Tjernström, M., Leaitch, W. R., and Abbatt, J. P. D.: Aerosol composition and sources in the central Arctic Ocean during ASCOS, Atmos. Chem. Phys., 11, 10619–10636, doi:10.5194/acp-11-10619-2011, 2011.

Chuang, P.: Measurement of the timescale of hygroscopic growth for atmospheric aerosols, J. Geophys. Res., 108, 4282, doi:10.1029/2002JD002757, 2003.

Davis, E. J.: A history and state-of-the-art of accommodation coefficients, Atmos. Res., 82, 561–578, 2006.

Draxler, R. R. and Rolph, G. D.: HYSPLIT (HYbrid Single-Particle Lagrangian Integrated Trajectory) Model access via NOAA ARL READY Website, available at: http://ready.arl.noaa.gov/HYSPLIT.php (last access: 7 April 2010), NOAA Air Resources Laboratory, Silver Spring, MD, 2011.

ACPD
14, 21223–21283, 2014

EANET (Acid Deposition Monitoring Network in East Asia): Report of the Inter-Laboratory Comparison Project 2007, available at: http://www.eanet.asia/product/, 2008.
Fu, P., Kawamura, K., Chen, J., and Barrie, L. A.: Isoprene, monoterpene, and sesquiterpene oxidation products in the high Arctic aerosols during late winter to early summer, Environ. Sci. Technol., 43, 4022–4028, 2009.
Miller, M. A. and Yuter, S. E.: Detection and characterization of heavy drizzle cells within subtropical marine stratocumulus using AMSR-E 89-GHz passive microwave measurements, Atmos. Meas. Tech., 6, 1–13, doi:10.5194/amt-6-1-2013, 2013.
Hede, T., Li, X., Leck, C., Tu, Y., and Ågren, H.: Model HULIS compounds in nanoaerosol clusters – investigations of surface tension and aggregate formation using molecular dynamics simulations, Atmos. Chem. Phys., 11, 6549–6557, doi:10.5194/acp-11-6549-2011, 2011.
Heintzenberg, J. and Leck, C.: The summer aerosol in the central Arctic 1991–2008: did it change or not?, Atmos. Chem. Phys., 12, 3969–3983, doi:10.5194/acp-12-3969-2012, 2012.
Heintzenberg, J., Birmili, W., Wiedensohler, A., Nowak, A., and Tuch, T.: Structure, variability and persistence of the submicrometer marine aerosol, Tellus B, 56, 357–367, 2004.
Heintzenberg, J., Leck, C., Birmili, W., Wehner, B., Tjernström, M., and Wiedensohler, A.: Aerosol number-size distributions during clear and fog periods in the summer high Arctic: 1991, 1996 and 2001, Tellus B, 58, 41–50, 2006.
Herman, G. and Goody, R.: Formation and persistence of summertime Arctic stratus clouds, J. Atmos. Sci., 33, 1537–1553, 1976.
Hinds, W. C.: Aerosol Technology: Properties, Behavior, and Measurement of Airborne Particles, Wiley-Interscience, 504 pp., ISBN: 978-0-471-19410-1, 1999.
Hoppel, W. A., Frick, G. M., and Larson, R. E.: Effect of nonprecipitating clouds on the aerosol size distribution in the marine boundary layer, Geophys. Res. Lett., 13, 125–128, 1986.
Hoppel, W. A., Frick, G. M., Fitzgerald, J. W., and Larson, R. E.: Marine boundary layer measurements of new particle formation and the effects non precipitating clouds have on aerosol size distribution, J. Geophys. Res., 99, 14443–14459, doi:10.1029/94JD00797, 1994.
Intrieri, J. M., Fairall, C. W., Shupe, M. D., Persson, P. O. G., Andreas, E. L., Guest, P. S., and Moritz, R. E.: An annual cycle of Arctic surface cloud forcing at SHEBA, J. Geophys. Res., 107, 8039, doi:10.1029/2000JC000439, 2002.
Karl, M., Leck, C., Coz, E., and Heintzenberg, J.; Marine nanogels as a source of atmospheric nanoparticles in the high Arctic, Geophys. Res. Lett., 40, 3738–3743, doi:10.1002/grl.50661, 2013.

ACPD
14, 21223–21283, 2014

Kay, J. E. and Gettelman, A.: Cloud influence on and response to seasonal Arctic sea ice loss, J. Geophys. Res., 114, D18204, doi:10.1029/2009JD011773, 2009.
Kerminen, V.-M. and Leck, C.: Sulfur chemistry over the central Arctic Ocean during the summer: gas-to-particle transformation, J. Geophys. Res., 106, 32087–32099, 2001.
Köhler, H.: The nucleus in and the growth of hygroscopic droplets, T. Faraday Soc., 32, 1152–1161, 1936.
Kupiszewski, P., Leck, C., Tjernström, M., Sjogren, S., Sedlar, J., Graus, M., Müller, M., Brooks, B., Swietlicki, E., Norris, S., and Hansel, A.: Vertical profiling of aerosol particles and trace gases over the central Arctic Ocean during summer, Atmos. Chem. Phys., 13, 12405–12431, doi:10.5194/acp-13-12405-2013, 2013.
Lannefors, H., Heintzenberg, J., and Hansson, H.-C.: A comprehensive study of physical and chemical parameters of the Arctic summer aerosol; results from the Swedish expedition Ymer-80, Tellus B, 35, 40–54, 1983.
Leaitch, W. R., Strapp, J. W., and Isaac, G. A.: Cloud droplet nucleation and cloud scavenging of aerosol sulfate in polluted atmospheres, Tellus B, 38, 328–344, 1986.
Leck, C. and Bigg, E. K.: Aerosol production over remote marine areas – a new route, Geophys. Res. Lett., 23, 3577–3581, 1999.
Leck, C. and Bigg, E. K.: Biogenic particles in the surface microlayer and overlaying atmosphere in the central Arctic Ocean during summer, Tellus B, 57, 305–316, 2005a.
Leck, C. and Bigg, E. K.: Evolution of the marine aerosol – a new perspective, Geophys. Res. Lett., 32, L19803, doi:10.1029/2005GL023651, 2005b.
Leck, C. and Bigg, E. K.: New particle formation of marine biological origin, Aerosol Sci. Tech., 44, 570–577, 2010.
Leck, C. and Persson, C.: Seasonal andshort-term variability in dimethyl sulfide, sulfur dioxide and biogenic sulfurand sea salt aerosol particles in the arctic marine boundary layer, during summer and autumn, Tellus B, 48, 272–299, 1996.
Leck, C., Bigg, E. K., Covert, D. S., Heintzenberg, J., Maenhaut, W., Nilsson, E. D., and Wiedensohler, A.: Overview of the atmospheric research program during the International Arctic Ocean Expedition of 1991 (IAOE-91) and its scientific results, Tellus B, 48, 136–155, 1996.
Leck, C., Nilsson, E. D., Bigg, E. K., and Bäcklin, L.: Atmospheric program on the Arctic Ocean Expedition 1996 (AOE-96): an overview of scientific goals, experimental approaches, and instruments, J. Geophys. Res., 106, 32051–32067, 2001.

ACPD
14, 21223–21283, 2014

Leck, C., Norman, M., Bigg, E. K., and Hillamo, R.: Chemical composition and sources of the high Arctic aerosol relevant for cloud formation, J. Geophys. Res., 107, 4135, doi:10.1029/2001JD001463, 2002.

Leck, C., Tjernström, M., Matrai, P., Swietlicki, E., and Bigg, K.: Can marine micro-organisms influence melting of the Arctic pack ice?, EOS T. Am. Geophys. Un., 85, 25–32, doi:10.1029/2004EO030001, 2004

Leck, C., Gao, Q., Mashayekhy Rad, F., and Nilsson, U.: Size-resolved atmospheric particulate polysaccharides in the high summer Arctic, Atmos. Chem. Phys., 13, 12573–12588, doi:10.5194/acp-13-12573-2013, 2013.

Lohmann, U. and Leck, C.: Importance of submicron surface-active organic aerosols for pristine Arctic clouds, Tellus B, 57, 261–268, 2005.

Martin, M., Chang, R. Y.-W., Sierau, B., Sjogren, S., Swietlicki, E., Abbatt, J. P. D., Leck, C., and Lohmann, U.: Cloud condensation nuclei closure study on summer arctic aerosol, Atmos. Chem. Phys., 11, 11335–11350, doi:10.5194/acp-11-11335-2011, 2011.

Mauritsen, T., Sedlar, J., Tjernström, M., Leck, C., Martin, M., Shupe, M., Sjogren, S., Sierau, B., Persson, P. O. G., Brooks, I. M., and Swietlicki, E.: An Arctic CCN-limited cloud-aerosol regime, Atmos. Chem. Phys., 11, 165–173, doi:10.5194/acp-11-165-2011, 2011.

Morita, A., Sugiyama, M., Kameda, H., Koda, S., and Hanson, D. R.: Mass accommodation coefficient of water: molecular dynamics simulation and revised analysis of droplet train/flow reactor experiment, J. Phys. Chem. B, 108, 9111–9120, 2004.

Narukawa, M., Kawamura, K., Li, S.-M., and Bottenheim, J. W.: Dicarboxylic acids in the Arctic aerosols and snowpacks collected during ALERT 2000, Atmos. Environ., 36, 2491–2499, 2002.

Nilsson, E. D., Rannik, Ü., Swietlicki, E., Leck, C., Aalto, P. P., Norman, M., and Zhou, J.: Turbulent aerosol number fluxes during theArctic Ocean Expedition 1996, Part II: A wind driven source of sub micrometeraerosol particles from the sea, J. Geophys. Res., 106, 32139–32154, 2001.

Ovadnevaite, J., Ceburnis, D., Martucci, G., Bialek, J., Monahan, C., Rinaldi, M., Facchini, M. C., Berresheim, H.,Worsnop, D. R., and O'Dowd, C.: Primary marine organic aerosol: a dichotomy of low hygroscopicity and high CCN activity, Geophys. Res. Lett., 38, L21806, doi:10.1029/2011GL048869, 2011.

ACPD
14, 21223–21283, 2014

Orellana, M. V., Matrai, P. A., Leck, C., Rauschenberg, C. D., Lee, A. M., and Coz, E.: Marine microgels as a source of cloud condensation nuclei in the high Arctic, P. Natl. Acad. Sci. USA, 108, 13612–13617, 2011.

Paatero, J., Vaattovaara, P., Vestenius, M., Meinander, O., Makkonen, U., Kivi, R., Hyvärinen, A., Asmi, E., Tjernström, M., and Leck, C.: Finnish contribution to the Arctic Summer Cloud Ocean Study (ASCOS) expedition, Arctic Ocean 2008, Geophysica, 45, 119–146, 2009.

Petters, M. D. and Kreidenweis, S. M.: A single parameter representation of hygroscopic growth and cloud condensation nucleus activity, Atmos. Chem. Phys., 7, 1961–1971, doi:10.5194/acp-7-1961-2007, 2007.

Pruppacher, H. R. and Klett, J. D.: Microphysics of Clouds and Precipitation, Kluwer Academic Publishers, Dordrecht, 1997.

Roberts, G. C. and Nenes, A.: A continuous-flow stream wise thermal-gradient CCN chamber for atmospheric measurements, Aerosol Sci. Technol., 39, 206–221, doi:10.1080/027868290913988, 2005.

Ruehl, C. R., Chuang, P. Y., and Nenes, A.: How quickly do cloud droplets form on atmospheric particles?, Atmos. Chem. Phys., 8, 1043–1055, doi:10.5194/acp-8-1043-2008, 2008.

Sedlar, J., Tjernström, M., Mauritsen, T., Shupe, M. D., Brooks, I. M., Persson, P. O. G., Birch, C. E., Leck, C., Sirevaag, A., and Nicolaus, M.: A transitioning Arctic surface energy budget: the impacts of solar zenith angle, surface albedo and cloud radiative forcing, Clim. Dynam., 37, 1643–1660, doi:10.1007/s00382-010-0937-5, 2011.

Shantz, N. C., Chang, R. Y.-W., Slowik, J. G., Vlasenko, A., Abbatt, J. P. D., and Leaitch, W. R.: Slower CCN growth kinetics of anthropogenic aerosol compared to biogenic aerosol observed at a rural site, Atmos. Chem. Phys., 10, 299–312, doi:10.5194/acp-10-299-2010, 2010.

Shupe, M. D., Persson, P. O. G., Brooks, I. M., Tjernström, M., Sedlar, J., Mauritsen, T., Sjogren, S., and Leck, C.: Cloud and boundary layer interactions over the Arctic sea ice in late summer, Atmos. Chem. Phys., 13, 9379–9399, doi:10.5194/acp-13-9379-2013, 2013.

Sierau, B., Chang, R. Y.-W., Leck, C., Paatero, J., and Lohmann, U.: Single-particle characterization of the high-Arctic summertime aerosol, Atmos. Chem. Phys., 14, 7409–7430, doi:10.5194/acp-14-7409-2014, 2014.

Svenningsson, B., Rissler, J., Swietlicki, E., Mircea, M., Bilde, M., Facchini, M. C., Decesari, S., Fuzzi, S., Zhou, J., Mønster, J., and Rosenørn, T.: Hygroscopic growth and critical super-

ACPD
14, 21223–21283, 2014

saturations for mixed aerosol particles of inorganic and organic compounds of atmospheric relevance, Atmos. Chem. Phys., 6, 1937–1952, doi:10.5194/acp-6-1937-2006, 2006.
Takahama, S. and Russell, L. M.: A molecular dynamics study of water mass accommodation on condensed phase water coated by fatty acid monolayers, J. Geophys. Res., 116, D02203, doi:10.1029/2010JD014842, 2011.
Tjernström, M., Leck, C., Persson, P. O., Jensen, M., Oncley, S., and Targino, A.: The summertime arctic atmosphere: meteorological measurements during the Arctic Ocean Experiment 2001 (AOE-2001), B. Am. Meteorol. Soc., 85, 1305–1321, 2004.
Tjernström, M., Sedlar, J., and Shupe, M. D.: How well do regional climate models reproduce radiation and clouds in the Arctic?, J. Appl. Meteorol. Clim., 47, 2405–2422, 2008.
Tjernström, M., Birch, C. E., Brooks, I. M., Shupe, M. D., Persson, P. O. G., Sedlar, J., Mauritsen, T., Leck, C., Paatero, J., Szczodrak, M., and Wheeler, C. R.: Meteorological conditions in the central Arctic summer during the Arctic Summer Cloud Ocean Study (ASCOS), Atmos. Chem. Phys., 12, 6863–6889, doi:10.5194/acp-12-6863-2012, 2012.
Tjernström, M., Leck, C., Birch, C. E., Bottenheim, J. W., Brooks, B. J., Brooks, I. M., Bäcklin, L., Chang, R. Y.-W., de Leeuw, G., Di Liberto, L., de la Rosa, S., Granath, E., Graus, M., Hansel, A., Heintzenberg, J., Held, A., Hind, A., Johnston, P., Knulst, J., Martin, M., Matrai, P. A., Mauritsen, T., Müller, M., Norris, S. J., Orellana, M. V., Orsini, D. A., Paatero, J., Persson, P. O. G., Gao, Q., Rauschenberg, C., Ristovski, Z., Sedlar, J., Shupe, M. D., Sierau, B., Sirevaag, A., Sjogren, S., Stetzer, O., Swietlicki, E., Szczodrak, M., Vaattovaara, P., Wahlberg, N., Westberg, M., and Wheeler, C. R.: The Arctic Summer Cloud Ocean Study (ASCOS): overview and experimental design, Atmos. Chem. Phys., 14, 2823–2869, doi:10.5194/acp-14-2823-2014, 2014.
Tuckermann, R.: Surface tension of aqueous solutions of water-soluble organic and inorganic compounds, Atmos. Environ., 41, 6265–6275, 2007.
Twomey, S.: Pollution and the planetary albedo, Atmos. Environ., 8, 1251–1256, 1974.
Verdugo, P.: Marine microgels, Ann. Rev. Marine Sci., 4, 375–400, doi:10.1146/annurev-marine-120709-142759, 2011.
Walsh, J., Kattsov, V., Chapman, W., Govorkova, V., and Pavlova, T.: Comparison of Arctic climate simulations by uncoupled and coupled global models, J. Climate, 15, 1429–1446, 2002.

ACPD
14, 21223–21283, 2014

Winkler, P. M., Vrtala A., Wagner, P. E., Kulmala, M., Lehtinen, K. E. J., and Vesala, T.: Mass and thermal accommodation during gas-liquid condensation of water, Phys. Rev. Lett., 93, 075701-1–075701-4, 2004.

Winkler, P. M., Vrtala, A., Rudolf, R., Wagner, P. E., Riipinen, I., Vesala, T, Lehtinen, K. E. J., Viisanen, Y., and Kulmala, M.: Condensation of water vapor: Experimental determination of mass and thermal accommodation coefficients, J. Geophys. Res., 111, D19202, doi:10.1029/2006JD007194, 2006.

Xin, L., Leck, C., Sun, L., Hede, T., Tu, Y., and Ågren, H.: Cross-linked polysaccharide assemblies in marine gels: an atomistic simulation, J. Phys. Chem. Lett., 4, 2637–2642, doi:10.1021/jz401276r, 2013.

Zhou, J., Swietlicki, E., Berg, O. H., Aalto, P. P., Hämeri, K., Nilsson E. D., and Leck, C.: Hygroscopic properties of aerosol particles over the central Arctic Ocean during summer, J. Geophys. Res., 106, 32111–32123, 2001.

ACPD
14, 21223–21283, 2014

Table 1. The 25th, 50th (median) and 75th percentile CCNC separately for open water (OW-1), marginal ice zone (MIZ-1) and pack ice (PI-1, 3, 6, 8, 9, 10, 13, and 15) measurements at 0.2 % SS (counter 1). Values are at STP. Also listed are information on sampling start–stop times and sample duration and of the air trajectory cluster and average DOI during the sampling time for each of the impactors.

Sample	Start time (UTC)	End time (UTC)	Sampling location	Trajectory-cluster	DOI	CCNC cm^{-3}	CCNC 25 % percentile cm^{-3}	CCNC 75 % percentile cm^{-3}	Missing aerosol fraction
OW-1	3 Aug 2008 13:28	4 Aug 2008 08:13	Open water		N/A	12.9	8.20	24.64	0.51
MIZ-1	4 Aug 2008 12:04	5 Aug 2008 12:12	Marginal ice zone		0	57.3	33.5	70.2	0.67
PI-1	12 Aug 2008 23:12	14 Aug 2008 07:42	Ice drift	1	2.5	17.4	1.8	31.7	0.46
PI-3	15 Aug 2008 15:44	16 Aug 2008 15:02	Ice drift	2	1.6	23.8	6.4	52.66	0.68
PI-6	19 Aug 2008 06:31	20 Aug 2008 06:27	Ice drift	1	4.6	29.4	15.5	45.70	0.68
PI-8	22 Aug 2008 01:10	23 Aug 2008 06:05	Ice drift	3	N/A	13.0	6.88	16.78	0.40
PI-9	23 Aug 2008 09:10	24 Aug 2008 10:04	Ice drift	2	1.2	30.1	25.8	32.8	0.56
PI-10	24 Aug 2008 15:00	25 Aug 2008 06:30	Ice drift	2	1.4	23.8	15.5	41.43	0.31
PI-13	27 Aug 2008 16:49	29 Aug 2008 16:48	Ice drift	4	6.1	44.3	30.9	47.9	0.76
PI-15	31 Aug 2008 19:50	1 Sep 2008 13:31	Ice drift	5	9.3	0.95	0.4	2.1	0.57

ACPD
14, 21223–21283, 2014

Table 2. Assumptions on the missing non-water soluble aerosol fraction used in the simulations.

Simulation	Illustration	Description
AD		Missing fraction behaves like internally mixed adipic acid; low water-solubility and moderate surface active.
PIN		Missing fraction behaves like internally mixed cis-pinonic acid; low water-solubility and highly surface active.
INSOL		Missing fraction behaves like a water-insoluble particle inside the droplets; no surface activity.
SOL		Missing fraction is assumed to be non-existent, only the determined chemical size distribution is used.
AD_ext		The analyzed part is externally mixed with an aerosol consisting of adipic acid.
PIN_ext		The analyzed part is externally mixed with an aerosol consisting of cis-pinonic acid.

ACPD
14, 21223–21283, 2014

Table 3. Assumptions on the missing non-water soluble aerosol fraction used in the simulations.with modified condensation accommodation coefficients.

Simulation	Illustration	Description
AC1		As the AD case, but with the condensation-accommodation coefficient set to 10^{-4}.
AC2		As the AD case, but with a variable condensation-accommodation coefficient, see text for details.

ACPD
14, 21223–21283, 2014

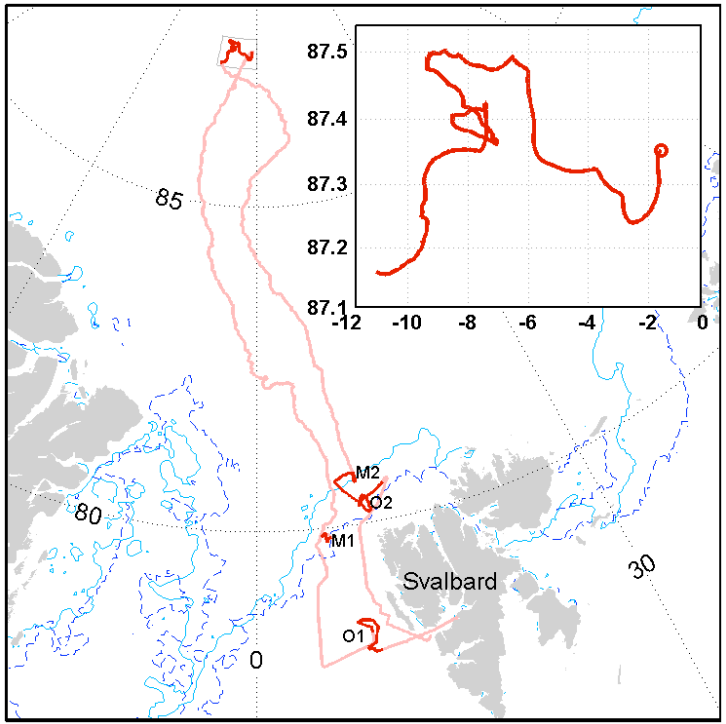

Figure 1. Map of the ASCOS cruise track (pink) with ice-drift period (PI-drift) highlighted (red) and (inset) shown in detail with the start of the drift marked by the circle. The left-hand part of the track shows the initial northward track while the right-hand track shows the southward, return track. Convoluted track lines in open water, OW (O1 and O2) and at the ice edge, MIZ (M1 and M2) are associated with shorter sampling stations. The dashed light blue line illustrates the ice edge at the time of entry and the darker blue line at the time of exit.

ACPD
14, 21223–21283, 2014

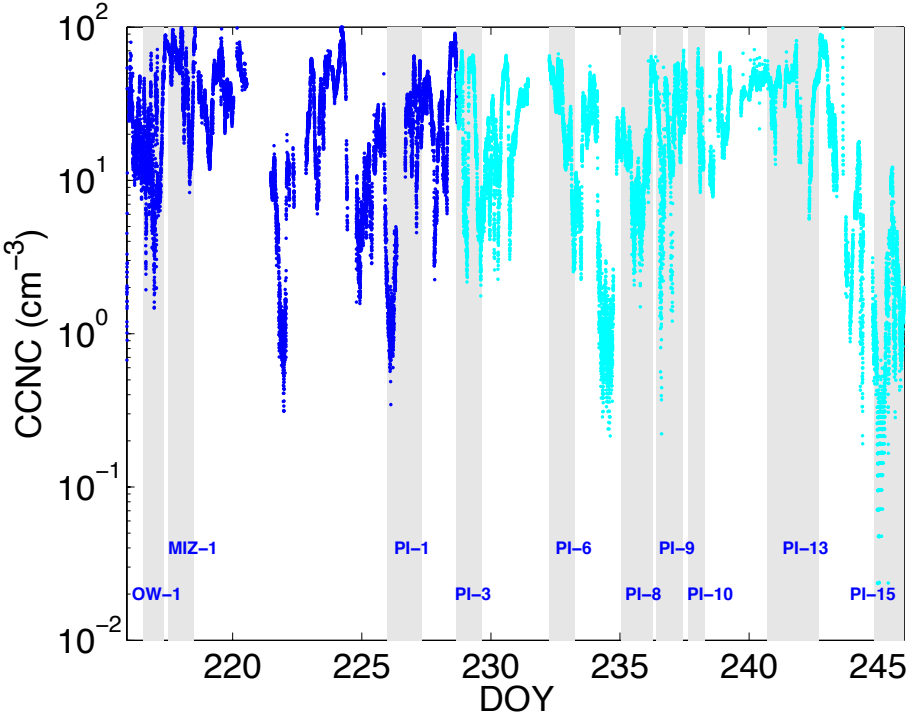

Figure 2. CCNC as a function of time in units of cm^{-3}. Blue dots show CCNC measured at 0.17 % water vapor SS, while light blue dots show the CCNC at 0.21 % water vapor supersaturation.

ACPD
14, 21223–21283, 2014

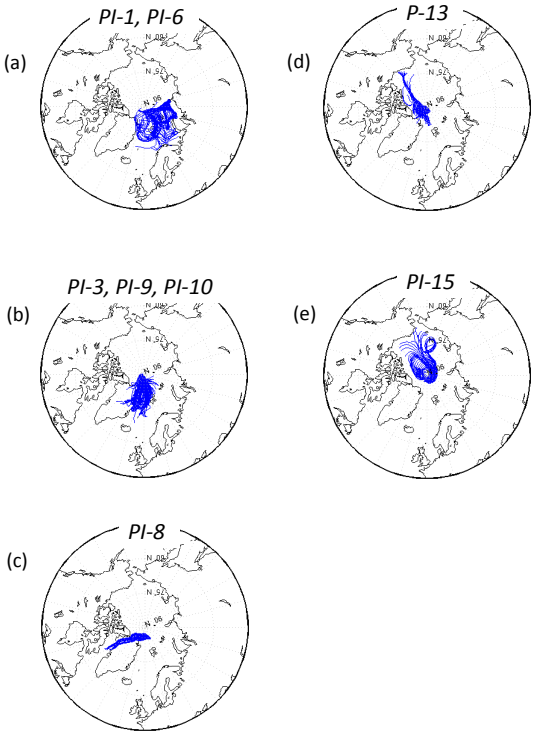

Figure 3. Air trajectory clusters with an arrival height of 100 m at the position of the icebreaker during: **(a)** cluster 1 (DOY 227, DOY 229–232) originated easterly from the Barents and Kara Seas, **(b)** cluster 2 (DOY 228, DOY 236, 238–239) from the Greenland Sea–Fram Strait area, **(c)** cluster 3 (DOY 234–235) from Greenland, **(d)** cluster 4 from north-western circumpolar over the pack ice during DOY 240–243, and **(e)** cluster 5 from north-western circumpolar over the pack ice during DOY 243–246.

ACPD
14, 21223–21283, 2014

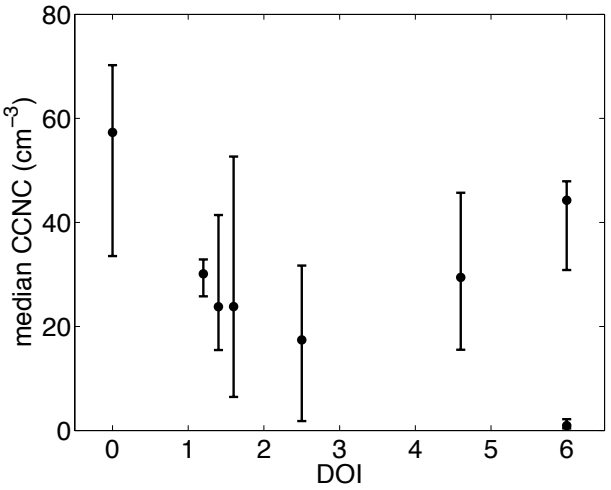

Figure 4. Median (50th percentile) CCCNC for the duration of the impactor samples as a function of travel time over ice (DOI, days). Data for all travel times of five days and longer have been collected at 6 days. Error bars indicate 25th and 75th percentile.

ACPD
14, 21223–21283, 2014

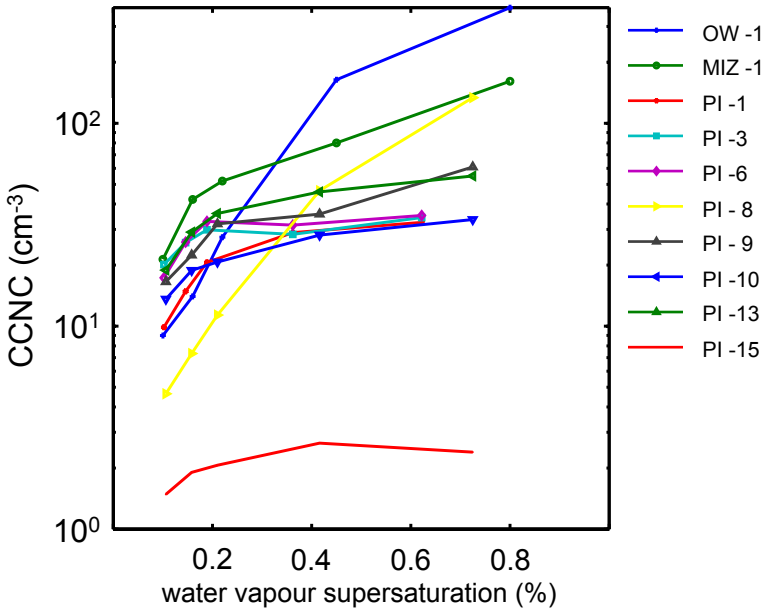

Figure 5. The measured CCNC as a function of the choice of water vapor SS (five levels between 0.1–0.8 %) as seen by the second CCN sampler. The data is shown separately for open water (OW 1), marginal ice zone (MIZ 1) and pack ice (PI-1, 3, 6, 8, 9, 10, 13, and 15) measurements.

ACPD
14, 21223–21283, 2014

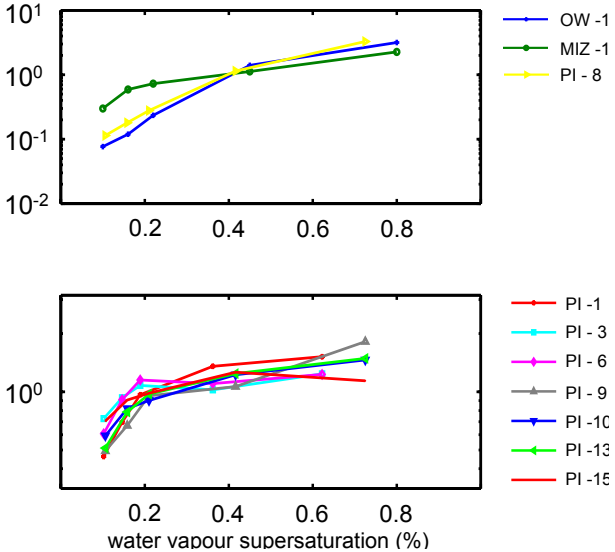

Figure 6. Variation in CCNC as a function of water vapor SS (as in Fig. 5) normalized to the average CCNC value for the duration of the impactor samples.

ACPD
14, 21223–21283, 2014

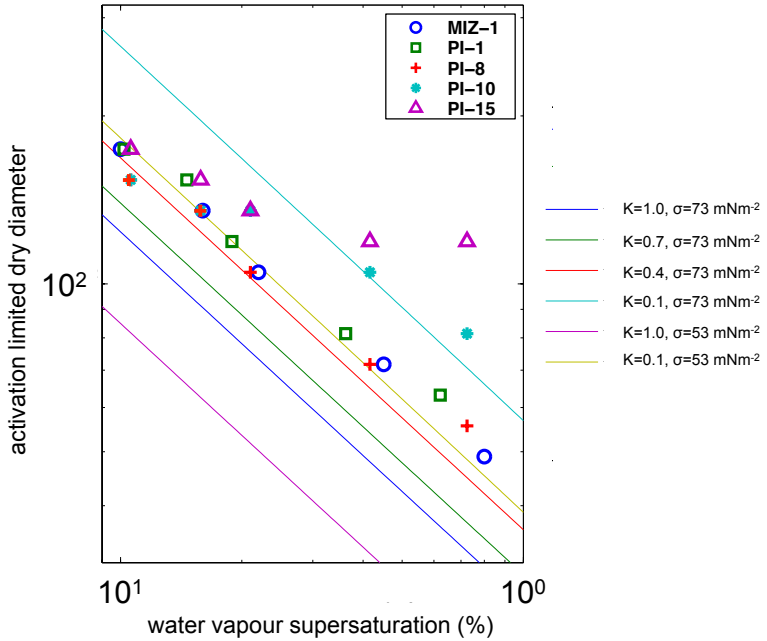

Figure 7. κ-Köhler theory prediction of the activation limit dry diameter for each of the impactor samples compared with experimental results.

ACPD
14, 21223–21283, 2014

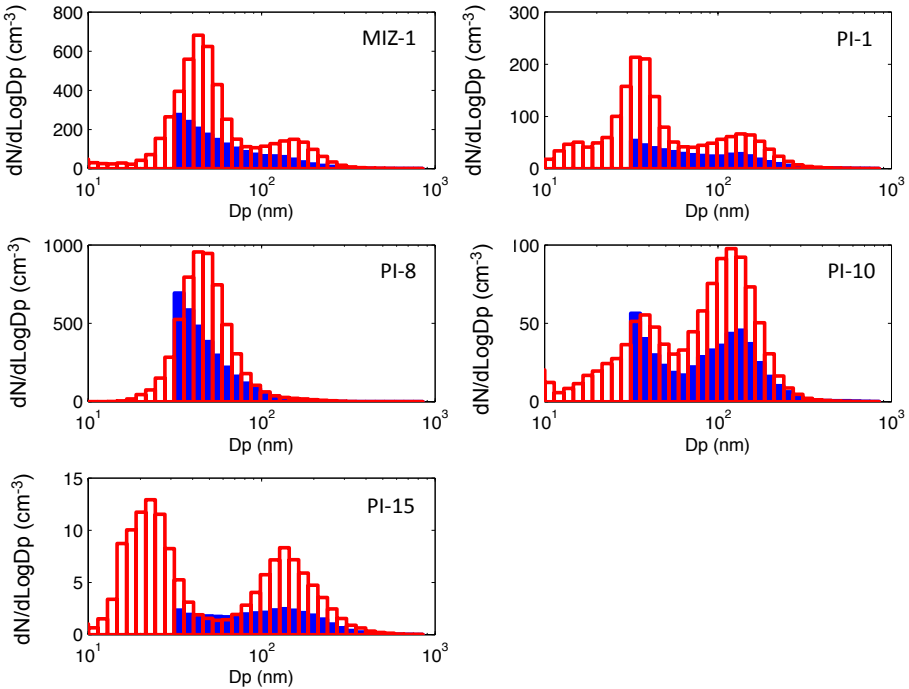

Figure 8. Comparison between TDMPS number size distribution (red) and converted mass size distributions (blue) for sample MIZ-1, PI-1, PI-8, PI-10 and PI-15.

ACPD
14, 21223–21283, 2014

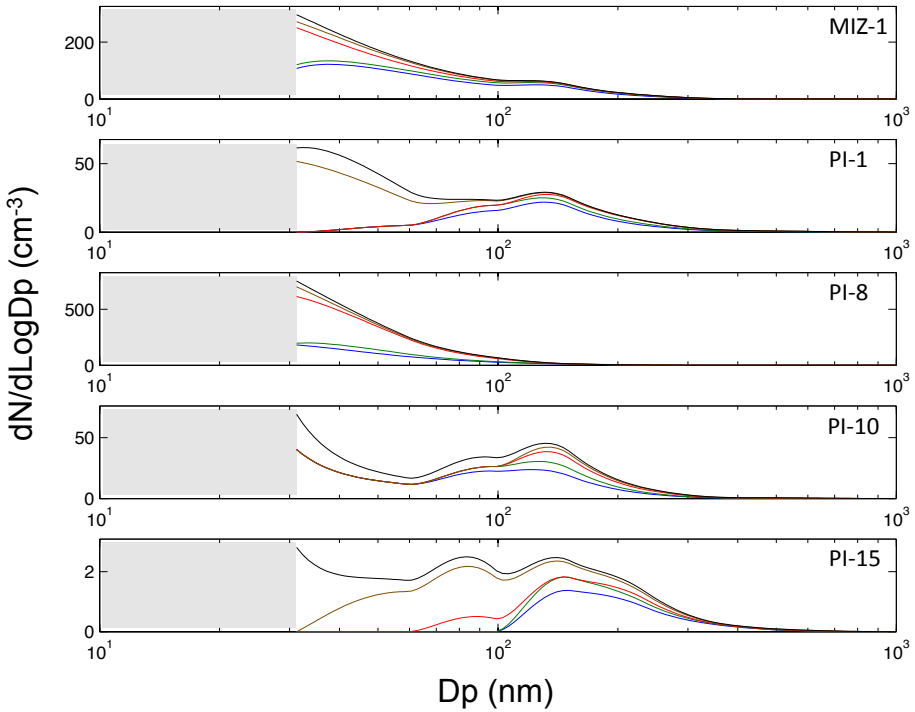

Figure 9. Number concentrations derived from impactor mass data. Blue line shows sulfate only, green lines sulfate + MSA, red lines sulfate + MSA + Na^+ + Cl^-, brown lines sulfate + MSA + Na^+ + Cl^- + Ca^{2+}, and black lines show the total analyzed concentration.

ACPD
14, 21223–21283, 2014

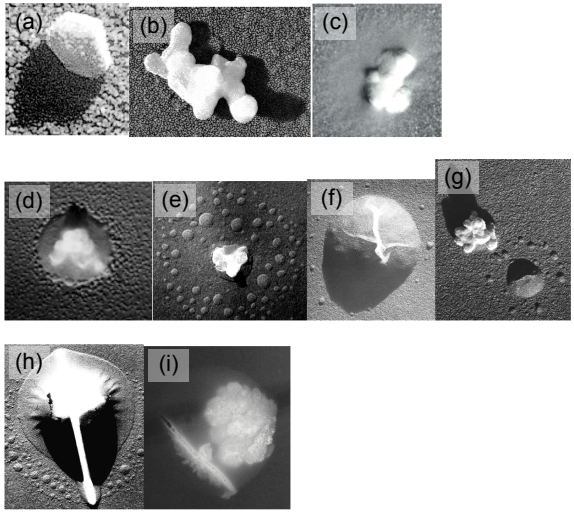

Figure 10. Examples of the changing nature of the high Arctic particles in different modal diameters: **(a–c)** sub-Aitken mode, **(a)** penta-hexagonal structure, crystalline and hydrophobic in nature assumed to be a colloidal building block of a polymer gel, **(b)** small polymer gel-aggregate slightly covered with hydrophilic mucus, **(c)** same as in **(b)** but with more mucus remaining promoting its hydrophilic properties, **(d–g)** Aitken to small accumulation mode, **(d)** particle with a high sulfuric acid content with a gel-aggregate inclusion embedded in a film of high organic content, **(e)** gel-aggregate with satellites, indicating the presence of organics and acids, **(f)** particle containing mainly ammonium sulfate and methane sulfonate, **(g)** external mixture of a gel-aggregate and similar particle as of **(f)** and (**h** and **i**) large accumulation mode, **(h)** sea-salt particle with an organic content. The rod through its centre is assumed to be a bacterium. The particle has an acquired coating of sulfuric acid, **(i)** a gel-aggregates containing a bacterium attached to a small aggregate possibly detached from the larger one. The particles bubble like shape indicates a possible recent injection to the atmosphere at the air sea interface.

ACPD
14, 21223–21283, 2014

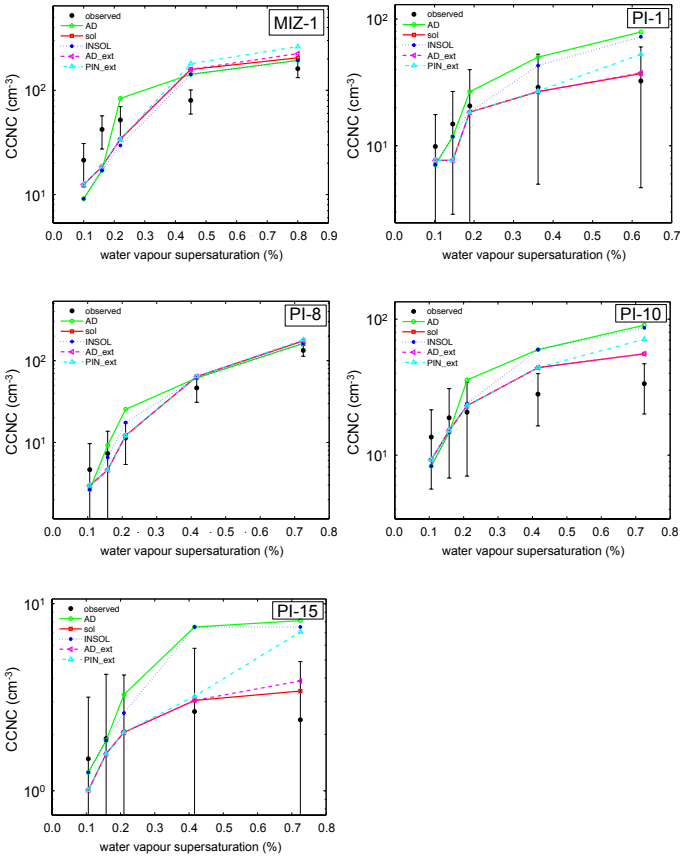

Figure 11. Observed and simulated CCNC for sample MIZ-1, PI-1, PI-8, PI-10 and PI-15, ranging from 0.1–0.8 % water vapor SS. Error bars represent one standard deviation.

ACPD
14, 21223–21283, 2014

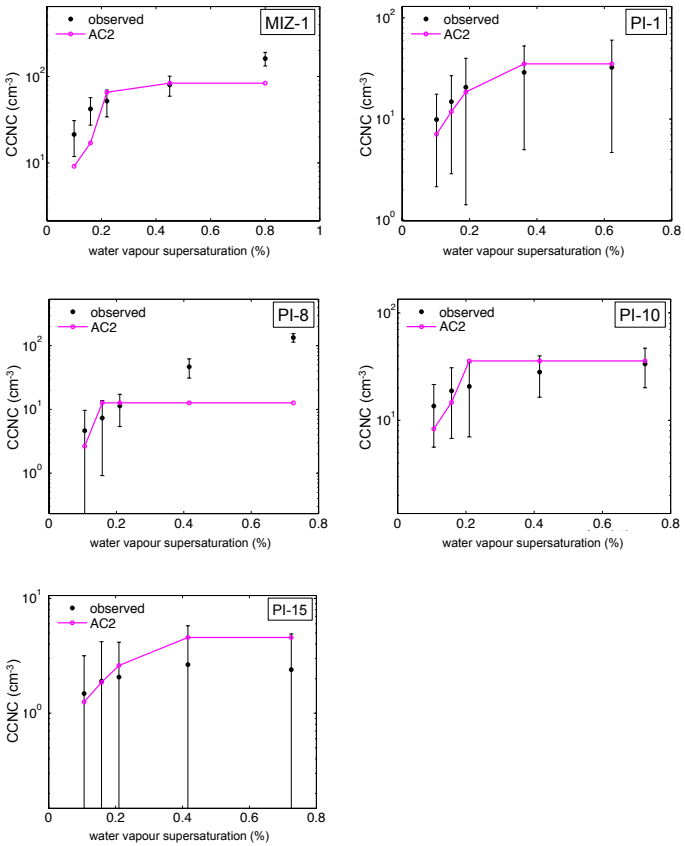

Figure 12. Observed and simulated CCNC for sample MIZ-1, PI-1, PI-8, PI-10 and PI-15, ranging from 0.1–0.8 % water vapor SS. Error bars represent one standard deviation. AC2 correspond to the assumption AD, see Table 2, with a variable condensation-accommodation coefficient.

ACPD
14, 21223–21283, 2014